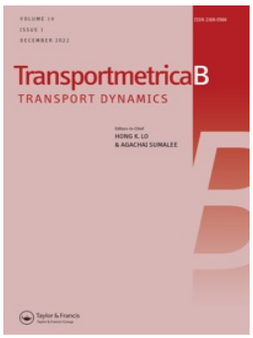

Transportmetrica B: Transport Dynamics

ISSN: 2168-0566 (Print) 2168-0582 (Online) Journal homepage: www.tandfonline.com/journals/ttrb20

How fast is still safe for truck platoons?

Shaoyu Sun, Wenbo Li, Boqun Zhang, Shuyou Yu, Hong Chen & Jung-Su Kim

To cite this article: Shaoyu Sun, Wenbo Li, Boqun Zhang, Shuyou Yu, Hong Chen & Jung-Su Kim (2026) How fast is still safe for truck platoons?, Transportmetrica B: Transport Dynamics, 14:1, 2648556, DOI: 10.1080/21680566.2026.2648556

To link to this article: https://doi.org/10.1080/21680566.2026.2648556

TRANSPORTMETRICA B: TRANSPORT DYNAMICS
2026, VOL. 14, NO. 1, 2648556
https://doi.org/10.1080/21680566.2026.2648556

Taylor & Francis
Taylor & Francis Group

RESEARCH ARTICLE

How fast is still safe for truck platoons?

Shaoyu Sun[a], Wenbo Li[a], Boqun Zhang[a], Shuyou Yu[a,b], Hong Chen[a,c] and Jung-Su Kim[d]

[a]The Department of Control Science and Engineering, Jilin University, Changchun, China; [b]The National Key Laboratory of Automotive Chassis Integration and Bionics, Jilin University, Changchun, China; [c]The College of Electronics and Information Engineering, Tongji University, Shanghai, China; [d]The Department of Electrical and Information Engineering, Seoul National University of Science and Technology, Seoul, South Korea

ABSTRACT

Truck platoons improve freight efficiency, but their high-speed safety under varying road conditions remains unclear. This study investigates the maximum safe speed of platoons by considering tire force saturation and longitudinal–lateral coupling. A hierarchical cooperative control framework is proposed, including cooperative control, control allocation, and action execution. A five-degree-of-freedom platoon model with lane-keeping is developed, and a distributed coupled sliding mode controller computes the desired tire forces. Feasible forces are obtained through constrained optimisation within tire limits, while steering angles and torques are derived from an inverse magic formula model. Finite-time convergence and string stability are theoretically guaranteed. Matlab/Simulink–TruckSim co-simulations show the proposed scheme improves platoon safety compared with decoupled methods. Furthermore, the maximum safe speed is quantified under different adhesion and curvature conditions. The results provide insights into the safe operating envelope of platoons and support their integration into intelligent transport systems.

ARTICLE HISTORY
Received 7 September 2025
Accepted 28 February 2026

KEYWORDS
Truck platoon; sliding mode control; longitudinal and lateral motion coupling; vehicle dynamics

1 Introduction

Truck platoon control is a key research area within vehicle-to-infrastructure (V2I) systems. Implementing truck platooning offers several advantages, including fuel savings, reduced collision risk, and improved road capacity (Li et al. 2023; Oriol et al. 2024). Current research on truck platoon control primarily focuses on managing both longitudinal and lateral motions. However, the nonlinear dynamics of trucks, characterised by strong coupling between longitudinal and lateral dynamics, tire nonlinearity, and tire force interactions, make the development of efficient and reliable controllers a critical area of ongoing research (Hua et al. 2025).

1.1 Motivation

Although extensive research has been conducted on truck platooning control, there are still several critical gaps. First, while many existing studies treat longitudinal and lateral control as separate problems, the interaction between these two dynamics becomes non-negligible under realistic driving conditions and can significantly influence overall vehicle stability and control performance. Second, some studies account for the coupling between longitudinal and lateral vehicle dynamics, they often neglect tire force saturation constraints, which play a critical role in limiting the achievable control forces under high-demand manoeuvres. Third, this study addresses the lack of systematic analysis in the existing literature by characterising the truck's maximum safe driving speed across different road curvatures and tire–road friction coefficients, thereby offering valuable guidance for speed planning under diverse operating conditions. These gaps highlight the necessity of developing a control framework that (i) simultaneously captures the coupling between longitudinal and lateral dynamics, (ii) explicitly incorporates tire force saturation constraints, and (iii) adapts the vehicle's speed to road curvature and friction variations to ensure safe and reliable operation under real-world driving conditions.

CONTACT Shuyou Yu shuyou@jlu.edu.cn The Department of Control Science and Engineering, Jilin University, Changchun, 130025, China

Motivated by these challenges, this work aims to establish a unified control and safety assessment framework that explicitly accounts for longitudinal–lateral coupling, tire saturation limits, and road-dependent speed feasibility in truck platoons. Specifically, a hierarchical cooperative control architecture is developed that is capable of generating dynamically feasible tire forces, ensuring finite-time convergence and string stability, and quantifying the maximum safe driving speed under varying curvature and adhesion conditions. The comparison between the proposed work and existing studies are summarised in Table 1. As summarised in the table, while some studies have focused on decoupled vehicle control and safety analysis (Dai, Wang, and Xie 2024; Yu, Sun, et al. 2025), they often overlook the coupled longitudinal–lateral dynamics and tire force saturation constraints. In contrast, several works have adopted model predictive control (MPC) to account for vehicle coupling effects (Feng et al. 2023a; Yu, Liu, et al. 2025). However, MPC typically requires an accurate model and imposes a higher computational burden compared to sliding mode control (SMC), especially when the model is complex. Other researchers have considered tire saturation under decoupled control frameworks (Liang et al. 2021; Zhang, Wang, and Wang 2023) or investigated tire force constraints together with safety analysis (Alonso, Mántaras, and Luque 2019). In comparison, the present work incorporates all three aspects-coupled dynamics, tire force saturation constraints, and systematic safety assessment-effectively bridging a critical gap in the existing research.

This work is most directly related to recent studies that also address coupled longitudinal–lateral platoon control, such as Feng et al. (2023a) and Yu, Sun, et al. (2025). However, it introduces several key distinctions and substantive advancements. Firstly, in terms of the control methodology, a finite-time sliding mode control scheme is employed, contrasting with the MPC approach used in Feng et al. (2023a). The SMC design offers superior computational efficiency and inherent robustness, which is advantageous for real-time implementation. Secondly, regarding tire force handling, our hierarchical framework features a dedicated control allocation layer that solves a constrained optimisation problem to ensure adherence to nonlinear tire-force limits, followed by an inverse 'magic formula' for execution. This provides a more direct and explicit enforcement of actuator constraints compared to the Koopman-linearised model used in Feng et al. (2023a). Most importantly, regarding the core objective, while the aforementioned studies primarily focus on tracking accuracy and stability, our work advances the field by leveraging the integrated control-structure to systematically quantify the maximum safe driving speed across different road conditions. This shifts the focus from 'how to drive' to 'how fast is safe to drive,' providing a concrete safety metric for operational guidance.

1.2 Related work

Distributed controllers are commonly employed in truck platoons, where each truck is equipped with its own control unit (Zhou et al. 2025). These distributed controllers coordinate the platoon by processing feedback from the leading truck and adjacent trucks. Research on distributed control in truck platoons has developed two main approaches. The first focuses on longitudinal control, managing acceleration and deceleration, but neglects the lateral control needed for turning and lane changing. The second assumes a constant longitudinal speed and focuses on the design of controllers for lateral motion.

In order to manage the longitudinal following system of truck platoons, an integral sliding mode control strategy combined with a disturbance observer is proposed as a means of mitigating position and acceleration uncertainties. Simulations demonstrate that this approach can ensure the string stability of the platoon within a finite time (Wang et al. 2019). In Wen and Guo (2021), a distributed hierarchical scheme for longitudinal motion control of vehicle platoons was developed. The framework aims to minimise inter-vehicle spacing errors, thereby facilitating convergence to the desired spacing. To address the inherent

Table 1. Comparing the proposed work with some previous studies.

Studies	Decoupled control	Coupled control	Tire force saturation	Safety analysis
Dai, Wang, and Xie (2024), Yu, Sun, et al. (2025)	√	×	×	√
Feng et al. (2023a), Yu, Liu, et al. (2025)	×	√	×	×
Liang et al. (2021), Zhang, Wang, and Wang (2023)	√	×	√	×
Alonso, Mántaras, and Luque (2019)	×	×	√	√
Proposed work	×	√	√	√

uncertainties in vehicle dynamics, a parameter adaptation law is incorporated into the controller. In Feng et al. (2023b), a hierarchical control strategy for the longitudinal motion of vehicle platoons was developed. The upper-layer employs a distributed model predictive controller with conditions that ensure string stability and impose terminal equality constraints for asymptotic consistency. The lower-layer utilises a control scheme that combines feedforward and feedback controllers to compensate for unmodeled dynamics and uncertainties. A novel γ-string stability concept is introduced for bidirectionally connected multi-objective vehicle platoons. A distributed economic model predictive control (DEMPC) algorithm is proposed to optimise both longitudinal tracking and fuel economy. Compared to traditional platoon control methods, the DEMPC algorithm demonstrates a 4.2% reduction in energy consumption while ensuring the completion of collaborative tasks (Luo et al. 2022). In Na and Cole (2022), an intelligent driver model was proposed to address safety concerns related to lateral lane changes. The model ensures lateral safety by introducing key constraints in lateral steering control, thereby improving vehicle lateral stability during lane changes and reducing the risks of skidding and rollover. In Lian et al. (2022), a nonlinear vehicle system model subjected to mixed network attacks was developed to address the lateral control issue of vehicles affected by external disturbances. A dynamic output feedback control method is proposed to achieve global exponential stability. In Goli and Eskandarian (2019), a model predictive control method is used to control the lateral motion of vehicle platoons, utilising a variable-spacing lateral reference trajectory and defining constraints and relaxation variables to quantify constraint violations, thereby ensuring lateral motion safety.

The above controllers are designed by considering either the longitudinal dynamics or the lateral dynamics of vehicle platoons separately. However, in real driving scenarios, the lateral dynamics of vehicles significantly affect their longitudinal dynamics, indicating a coupling between the two motions (Xu et al. 2015). The design of controllers for longitudinal or lateral dynamics often leads to inaccuracies, which makes it challenging to ensure the safety of the platoon under complex operating conditions. In Kim, Park, and Jhang (2020), a novel inter-vehicle spacing strategy and a three-degree-of-freedom longitudinal–lateral decoupling error dynamics model were proposed to ensure the driving safety of the platoon without utilising longitudinal trajectories, with simulation experiments conducted in 12 different scenarios. In Manuel et al. (2022), a model predictive controller for vehicle platoons was proposed, which considers both lateral and longitudinal dynamics. The controller is utilised to achieve steering and driving for autonomous vehicles, thereby ensuring their safety. In Latrech et al. (2018), an integrated longitudinal and lateral control method based on a wireless communication network within a vehicle platoon was proposed, aiming to ensure that the platoon remains within a designated lane. The longitudinal controller is designed to ensure stability and robustness while considering actuator saturation constraints and controller limitations during the design process. The lateral control employs a multi-fuzzy control approach, which is formulated using linear matrix inequalities. In Rajamani et al. (2000), a coordinated control system is developed that considers both longitudinal and lateral dynamics. The longitudinal control ensures that each following vehicles maintain a safe distance, while the lateral control keeps the vehicles within the lane, thus enabling vehicles to travel in a tight platoon. A robust $H - \infty$ platoon controller is designed for heterogeneous vehicle platoons travelling on roads with varying slopes and air resistance, and experiencing communication delays (Xu et al. 2019). The concept of L_2 string stability is defined in order to ensure that disturbances do not grow indefinitely as they propagate through the platoon. Simulations validate the controller effectiveness in ensuring stability for both longitudinal and lateral dynamics. In Yu et al. (2022), the coupling characteristics of longitudinal and lateral vehicle dynamics are simultaneously considered. The Koopman operator theory is employed to approximate the three-degree-of-freedom vehicle dynamics model. A hierarchical control scheme is proposed, where the upper layer employs a model predictive control strategy, and the lower layer converts the desired control actions into throttle angles, brake pressures, and front wheel steering angles through an inverse dynamics model. The effectiveness of the controller is validated through simulations. In Feng et al. (2023a) the dynamics of commercial truck platoons are considered. To this end, a five-degree-of-freedom (5-DOF) coupled longitudinal–lateral dynamics model and a nonlinear tire model are employed. The Koopman operator theory is employed to obtain a linear model. A predictive controller is designed to reduce the computational burden and guarantee the real-time performance of the controller.

Sliding mode control has demonstrated remarkable robustness to system parameter variations and external disturbances. This is attributed to its ability to handle uncertainty and disturbances in nonlinear systems. As a

result, it has been widely applied in control strategies for vehicle platoons recently. In Ali, Garcia, and Martinet (2013), the constant-time headway strategy was modified, and sliding mode controllers were independently designed for longitudinal and lateral dynamics. The effectiveness of this approach is validated through real-world vehicle tests on urban roads. In Guo and Zhao (2023), the potential impact of model parameter uncertainties and unknown disturbances is taken into account. Considering the communication topologies of predecessor-following and bidirectional, two nonlinear terminal sliding mode control and distributed cooperative control algorithms have been proposed. These algorithms guarantee the string stability of the platoon and robustness within the system. In Li et al. (2022), the impact of communication delays on platoon control was addressed, and a sliding mode control strategy utilising global dynamic information and graph theory was proposed. In Zhu et al. (2024), a finite-time-based sliding-mode controller and disturbance observer for connected vehicle platoon with uncertain dynamics were proposed, and the proposed controller was verified by extensive simulations and co-simulations, and small-scaled experiments.

In the practical engineering applications of truck platoons, the rapid convergence of platoon errors is a critical characteristic (Hong, Huang, and Xu 2001). The finite-time convergence theory of sliding mode control demonstrates that the errors within the platoon can rapidly converge to the desired range, thereby ensuring the stability and reliability of the platoon (Sun et al. 2017). In Qiao and Zhang (2019), the slow convergence speed of nonsingular integral terminal sliding mode (NITSM) control when far from the equilibrium point is considered, and an adaptive fast nonsingular integral terminal sliding mode control method is proposed as a solution. This method ensures rapid transient convergence, both when the system is far from and close to the equilibrium point, thereby enhancing the convergence speed of the existing NITSM. In Aghababa and Saif (2020), a robust terminal sliding mode controller was proposed to improve the convergence speed of platoon errors. This controller ensures finite-time stability for each vehicle in the platoon and guarantees the string stability of the platoon.

1.3 Contributions

To address the safety control problem of truck platoons, a finite-time distributed sliding mode control strategy is proposed. The main contributions of this paper are summarised as follows.

(1) A hierarchical control scheme and a finite-time sliding mode coupled control law are designed considering the lateral and longitudinal dynamics of the truck. The finite-time reachability of the designed controller and the string stability of the platoon are proved theoretically.
(2) The tire is the only interface between the truck and the road. Its nonlinear characteristics, particularly under large slip angles or high lateral forces, have a significant impact on truck stability and control performance. This work distinguishes itself from many existing studies by explicitly considering tire nonlinearity and tire force constraints, which are often neglected in simplified tire models. Therefore, incorporating these realistic tire characteristics into the modeling and control scheme is essential to ensure the safety of a truck platoon, especially under varying road adhesion coefficients and road curvatures.
(3) This study compares the performance between coupled and decoupled control strategies. The results show that the maximum safe driving speed of a truck platoon with distributed coupled controllers is increased under different road adhesion coefficients and road curvatures. The study further quantifies and analyses the maximum safe driving speed of the platoon under different road adhesion coefficients and road curvatures.

1.4 Paper organisation

The paper proceeds as follows: In Section 2, a 5-DOF truck dynamics model and a lane-keeping model are introduced. In Section 3, a hierarchical control scheme including a cooperative control, a control allocation, and an action execution layer is developed. The finite-time reachability and the string stability of truck platoons are analysed. In Section 4, simulation experiments under different scenarios are provided. Section 5 concludes the paper.

2 Problem formulation

Consider a truck platoon consisting of $N + 1$ homogeneous trucks traveling along a road, where the leading truck is denoted by 0 and the following trucks are $1\cdots N$, respectively. Suppose that the leading truck is driven by a human driver along the desired path. The purpose of this paper is to design distributed controllers for the following trucks, ensuring the safe travel of the entire platoon. In this paper, the constant spacing policy (Yu and Yeo 2025) and the predecessor–leader following information flow topology (Cui et al. 2024; Yu, Hua, and Wang 2023) are adopted.

2.1 Five-degree-of-freedom dynamics model of trucks

A 5-DOF dynamics model is employed, which considers the longitudinal and lateral coupling characteristics (Shi et al. 2017). As illustrated in Figure 1, the 5-DOF dynamics model of trucks includes longitudinal motion, lateral motion, yaw motion, and the rolling of the front and rear wheels. The control inputs include the driving torques on the front and rear wheels, and the steering angle of the front wheels.

The 5-DOF dynamics model of the truck can be expressed as follows:

$$\begin{cases} \dot{v}_x = \frac{1}{m}(F_{xf}\cos\delta_f - F_{yf}\sin\delta_f + F_{xr} - F_{wx}) + v_y\omega \\ \dot{v}_y = \frac{1}{m}(F_{xf}\sin\delta_f + F_{yf}\cos\delta_f + F_{yr} - F_{wy}) - v_x\omega \\ \dot{\omega} = \frac{1}{I_z}(aF_{xf}\sin\delta_f + aF_{yf}\cos\delta_f - bF_{yr}) \\ \dot{\omega}_f = \frac{1}{J_f}(T_{df} - RF_{xf}) \\ \dot{\omega}_r = \frac{1}{J_r}(T_{dr} - RF_{xr}) \end{cases}, \tag{1}$$

where v_x, v_y and ω denote the longitudinal velocity, lateral velocity, and yaw angle rate of the truck, respectively. The terms ω_f and ω_r represent the angular velocities of the front and rear wheels, m represents the total mass of the truck, and I_z represents the moment of inertia around the yaw axis. The distances from the centre of mass to the front and rear axles are denoted by a and b, respectively. The terms J_f and J_r represent the moments of inertia of the front and rear wheels, respectively. The term δ_f represents the steering angle of the front wheel, while T_{df} and T_{dr} represent the torques of the front and rear wheels, respectively. The terms F_{xf}, F_{xr}, F_{yf} and F_{yr} denote the longitudinal forces of the front wheel, the longitudinal forces of the rear wheel, the lateral forces of the front wheel and the lateral forces of the rear wheel,

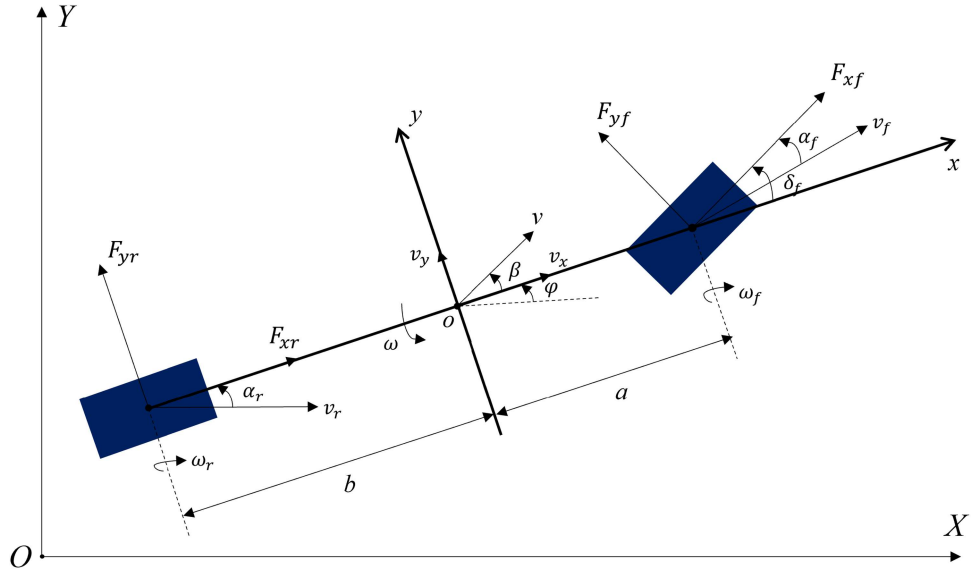

Figure 1. 5-DOF dynamics model of truck.

respectively. The terms F_{wx} and F_{wy} represent the effects of longitudinal and lateral air resistance, respectively. The term R is the wheel rolling radius. Note that a sign function is used to describe the air resistance (Chen et al. 2024), and the terms F_{wx} and F_{wy} can be calculated as follows:

$$\begin{cases} F_{wx} = \frac{1}{2}\rho C_x A_x v_x^2 \cdot \mathrm{sgn}(v_x) \\ F_{wy} = \frac{1}{2}\rho C_y A_y v_y^2 \cdot \mathrm{sgn}(v_y) \end{cases}, \tag{2}$$

where C_x and C_y represent the longitudinal and lateral air resistance coefficients, respectively. The terms A_x and A_y represent the longitudinal and lateral windward areas, respectively, and ρ represents the air density.

2.2 'Magic formula' tire model

The nonlinear characteristics of tires significantly influence the driving stability of platoons. This paper employs the 'magic formula' tire model to describe the characteristics of tires (Barbaro et al. 2024):

$$y = D \sin\left(C \arctan\left(Bx - E\left(Bx - \arctan Bx\right)\right)\right), \tag{3}$$

where B, C, D and E are the parameters of the tire. Note that in Equation (3), the term of x represents the slip ratio or the slip angle, and y corresponds to the longitudinal tire force or the lateral tire force, respectively.

Remark 1. The parameters B, C, D, and E of tires in the 'magic formula' tire model are fitting parameters, depending on road adhesion coefficient and vertical load (Dell'Orto et al. 2024), which need to be obtained by means of curve fitting.

The slip ratios of the front and rear tires are:

$$\begin{cases} k_f = \frac{\omega_f R - v_{xf}}{|v_{xf}|} \\ k_r = \frac{\omega_r R - v_{xr}}{|v_{xr}|} \end{cases}, \tag{4}$$

and the slip angles of the front and rear tires are (Hashemi and Khajepour 2024):

$$\begin{cases} \alpha_f = \delta_f - \arctan\left(\frac{v_y + a\omega}{v_x}\right) \\ \alpha_r = -\arctan\left(\frac{v_y - b\omega}{v_x}\right) \end{cases}. \tag{5}$$

Terms of v_{xf} and v_{xr} are the longitudinal velocity of the front and rear tires, v_{yf} and v_{yr} are the lateral velocity of the front and rear tires, which can be calculated:

$$\begin{cases} v_{xf} = v_x \cos\delta_f + (v_y + a\omega)\sin\delta_f \\ v_{yf} = -v_x \sin\delta_f + (v_y + a\omega)\cos\delta_f \\ v_{xr} = v_x \\ v_{yr} = v_y - b\omega \end{cases}. \tag{6}$$

When the value of the variable δ_f is small, such that $\cos\delta_f \approx 1, \sin\delta_f \approx \delta_f \approx 0$, Equation (6) can be simplified:

$$\begin{cases} v_{xf} = v_{xr} = v_x \\ v_{yf} = v_y + a\omega \\ v_{yr} = v_y - b\omega \end{cases}. \tag{7}$$

Under longitudinal and lateral tire forces during vehicle motion, the resultant force vector is constrained by the boundary μF_z, where μ is the road adhesion coefficient and F_z denotes the vertical load of the truck. To characterise this interaction, the tire mixed-slip model can be expressed as (Shi et al. 2017):

$$\begin{cases} F_{xf} = F_{xf0} \cdot \cos\left(\arctan\left(B_{g,x}(\alpha)\cdot\alpha\right)\right) \\ F_{yf} = F_{yf0} \cdot \cos\left(\arctan\left(B_{g,y}(k)\cdot k\right)\right) \\ F_{xr} = F_{xr0} \cdot \cos\left(\arctan\left(B_{g,x}(\alpha)\cdot\alpha\right)\right) \\ F_{yr} = F_{yr0} \cdot \cos\left(\arctan\left(B_{g,y}(k)\cdot k\right)\right) \\ B_{g,x}(\alpha) = r_{x,1} \cdot \cos\left(\arctan\left(r_{x,2}\cdot k\right)\right) \\ B_{g,y}(k) = r_{y,1} \cdot \cos\left(\arctan\left(r_{y,2}\cdot\alpha\right)\right) \end{cases}, \tag{8}$$

where F_{xf0}, F_{yf0}, F_{xr0} and F_{yr0} represent the steady-state longitudinal force of the front wheel, the steady-state lateral force of the front wheel, the steady-state longitudinal force of the rear wheel, and the steady-state lateral force of the rear wheel, respectively. The terms $B_{g,x}(\alpha)$ and $B_{g,y}(k)$ are the correction functions, while $r_{x,1}$, $r_{x,2}$, $r_{y,1}$ and $r_{y,2}$ denote the tire mixing slip coefficients.

Remark 2. The small-angle assumption in Equation (7) is imposed only at the cooperative control layer to enable finite-time stability guarantees. Importantly, it should not be interpreted as an operational restriction on the vehicles. From a safety perspective, truck platoons are expected to operate within small steering-angle regimes, however, practical disturbances inevitably drive the system outside this idealised region. The proposed hierarchical architecture is designed to remain valid: while the cooperative layer relies on simplified assumptions, the control allocation and execution layers employ full nonlinear tire and dynamic models, and the final steering commands are obtained via the nonlinear inverse 'magic formula' under explicit friction-ellipse constraints.

2.3 Platoon model

In this paper, a lane-keeping model for a truck platoon is employed, as illustrated in Figure 2, which captures the longitudinal position information between trucks in the platoon, the lateral position information of the trucks relative to the lane markings, and the angular information regarding the direction of travel (Zhou et al. 2023).

The longitudinal position and speed of the leading truck are denoted by $x_0(t)$ and $v_{x,0}(t)$, respectively.

For the ith truck in the platoon, its longitudinal position and speed are denoted by $x_i(t)$ and $v_{x,i}(t)$, respectively.

The constant spacing policy is used to define the longitudinal position error of the ith following truck relative to the $(i-1)$th following truck in the platoon (Karafyllis, Theodosis, and Papageorgiou 2023):

$$e_i(t) = x_i(t) - (x_{i-1}(t) - L), \tag{9}$$

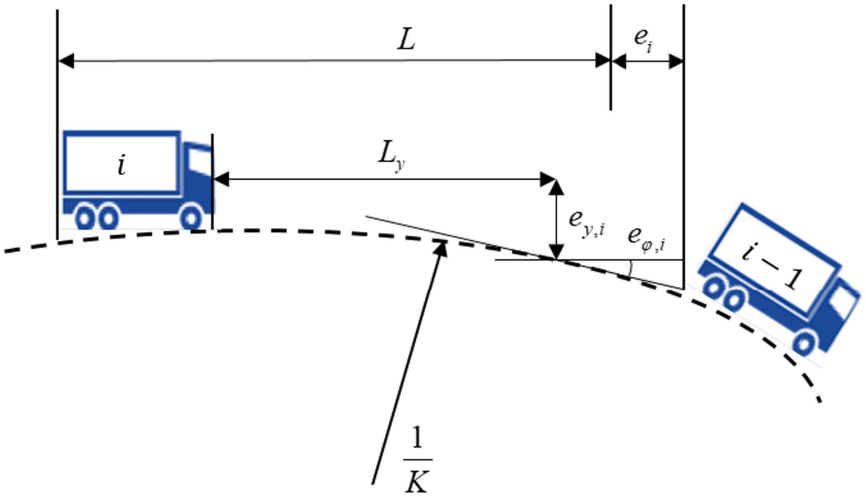

Figure 2. The lane-keeping model of a truck platoon.

where the desired inter-truck spacing, including the length of the truck, is denoted by L with $L = 20$ m. The longitudinal spacing error of the ith following truck relative to the leading truck in the platoon is defined as:

$$e_{i,0}(t) = x_i(t) - (x_0(t) - iL). \tag{10}$$

In terms of Equations (9) and (10), one has:

$$e_{i,0}(t) = e_1(t) + e_2(t)\ldots + e_i(t). \tag{11}$$

The combined longitudinal spacing error of the ith following truck in the platoon is defined as:

$$e_{x,i}(t) = \sigma_1 e_{i,0}(t) + \sigma_2 e_i(t), \tag{12}$$

where σ_1 and σ_2 are the weighting factors, and $\sigma_1 + \sigma_2 = 1$.

By taking the derivative of Equation (12), one has:

$$\dot{e}_{x,i}(t) = v_{x,i}(t) - \sigma_1 v_{x,0}(t) - \sigma_2 v_{x,i-1}(t). \tag{13}$$

To describe the lateral motion of a truck relative to the lane centreline, $e_{y,i}(t)$ is defined as the lateral position error of the truck from the centreline of the lane, and $e_{\varphi,i}(t)$ is the yaw angle error, which can be expressed as:

$$\begin{cases} \dot{e}_{y,i}(t) = v_{x,i}(t) e_{\varphi,i}(t) - v_{y,i}(t) - L_y \omega_i(t) \\ \dot{e}_{\varphi,i}(t) = \omega_{d,i}(t) - \omega_i(t) \end{cases}, \tag{14}$$

where the specified look-ahead distance, denoted by L_y, is set to 15 m. The yaw angle rate, denoted by $\omega_i(t)$, is compared to the desired yaw angle rate of the truck, defined as $\omega_{d,i}(t) = K v_{x,i}(t)$, where K is the road curvature.

Thus, the lane-keeping model for a truck platoon can be represented as:

$$\begin{cases} \dot{e}_{x,i}(t) = v_{x,i}(t) - \sigma_1 v_{x,0}(t) - \sigma_2 v_{x,i-1}(t) \\ \dot{e}_{y,i}(t) = v_{x,i}(t) e_{\varphi,i}(t) - v_{y,i}(t) - L_y \omega_i(t) \\ \dot{e}_{\varphi,i}(t) = \omega_{d,i}(t) - \omega_i(t) \end{cases}. \tag{15}$$

By combining, the platoon model can be expressed as:

$$\begin{cases} \dot{v}_{x,i}(t) = \frac{1}{m}(\Delta_{x,i}(t) - F_{wx,i}(t)) + v_{y,i}(t)\omega_i(t) \\ \dot{v}_{y,i}(t) = \frac{1}{m}(\Delta_{y,i}(t) - F_{wy,i}(t)) - v_{x,i}(t)\omega_i(t) \\ \dot{\omega}_i(t) = \frac{1}{I_z}\Delta_{\varphi,i}(t) \\ \dot{\omega}_{f,i}(t) = \frac{1}{J_f}(T_{df,i}(t) - RF_{xf,i}(t)) \\ \dot{\omega}_{r,i}(t) = \frac{1}{J_r}(T_{dr,i}(t) - RF_{xr,i}(t)) \\ \dot{e}_{x,i}(t) = v_{x,i}(t) - \sigma_1 v_{x,0}(t) - \sigma_2 v_{x,i-1}(t) \\ \dot{e}_{y,i}(t) = v_{x,i}(t) e_{\varphi,i}(t) - v_{y,i}(t) - L_y \omega_i(t) \\ \dot{e}_{\varphi,i}(t) = \omega_{d,i}(t) - \omega_i(t) \end{cases}. \tag{16}$$

The term of $\Delta_i(t) = [\Delta_{x,i}(t), \Delta_{y,i}(t), \Delta_{\varphi,i}(t)]^T$ represents the resultant forces derived from the front and rear longitudinal and lateral tire forces. The expressions are as follows:

$$\begin{cases} \Delta_{x,i}(t) = F_{xf,i}(t) + F_{xr,i}(t) \\ \Delta_{y,i}(t) = F_{yf,i}(t) + F_{yr,i}(t) \\ \Delta_{\varphi,i}(t) = aF_{yf,i}(t) - bF_{yr,i}(t) \end{cases}. \tag{17}$$

The state of the ith truck in the platoon is defined as $X_i = [v_{x,i}(t), v_{y,i}(t), \omega_i(t), \omega_{f,i}(t), \omega_{r,i}(t)]^T$, representing its longitudinal speed, lateral speed, yaw angle rate, and angular velocities of the front and rear wheels

of the ith truck. Denote $E(t) = [e_{x,i}(t), e_{y,i}(t), e_{\varphi,i}(t)]^T$, which represents the longitudinal spacing error, lateral position error, and yaw angle error of the ith following truck. Furthermore, the control input of the ith truck is defined as $U_i(t) = [T_{df,i}(t), T_{dr,i}(t), \delta_{f,i}(t)]^T$, representing the front wheel drive torque, rear wheel drive torque, and front wheel angle.

2.4 Longitudinal string stability for truck platoon

String stability: When a truck platoon is subject to unknown disturbances, the position errors are not amplified along the platoon, that is:

$$\|G_i(s)\| = \left\| \frac{e_i(s)}{e_{i-1}(s)} \right\|_\infty \leq 1, \tag{18}$$

where term of $G_i(s)$ represents the transfer function of the longitudinal error, $e_i(s)$ and $e_{i-1}(s)$ denote the Laplace transform of $e_i(t)$ and $e_{i-1}(t)$, respectively.

Remark 3. Note that the definition of string stability is established in the frequency domain, i.e. reflecting the steady-state behaviour of the platoon only.

2.5 Control objectives of truck platoon

A distributed control scheme is proposed for cooperative a truck platoon with the following control objectives:

(1) Longitudinal finite-time consensus: The speed of the ith following truck tracks the speed of the leading truck within finite time, and it aims to maintain the desired following spacing between adjacent trucks, which can be formulated as:

$$\begin{cases} \lim\limits_{t \to t_{x,i}} \|e_{x,i}(t)\| = 0 \\ \lim\limits_{t \to t_{x,i}} \|e_{v,i}(t)\| = 0 \end{cases}, \tag{19}$$

where $e_{v,i}(t)$ denotes the longitudinal speed error of the ith following truck.

(2) The perturbation does not amplify as it propagates towards the tail of the platoon, i.e. the entire platoon exhibits string stability.
(3) Lateral finite-time stability: The objective of lateral control in the truck platoon is to ensure that trucks travel along the centreline of the road. And the lateral position error and heading angle error of the ith following truck are converged to zero in finite time:

$$\begin{cases} \lim\limits_{t \to t_{y,i}} \|e_{y,i}(t)\| = 0 \\ \lim\limits_{t \to t_{y,i}} \|e_{\varphi,i}(t)\| = 0 \end{cases}. \tag{20}$$

3 Controller design

Considering the coupled dynamics of trucks and the nonlinearity of tires, this paper constructs a hierarchical control scheme, which aims to coordinate longitudinal and lateral control and includes a cooperative control layer, a control allocation layer, and an action execution layer. In the cooperative control layer, a finite-time distributed sliding mode controller is used to derive the expected longitudinal and lateral tire forces. In the control allocation layer, optimisation problems are solved based on tire force constraints to determine these expected forces. In the action execution layer, the control inputs for the trucks are obtained through the 'magic formula' tire model and torque formula: the expected front and rear wheel

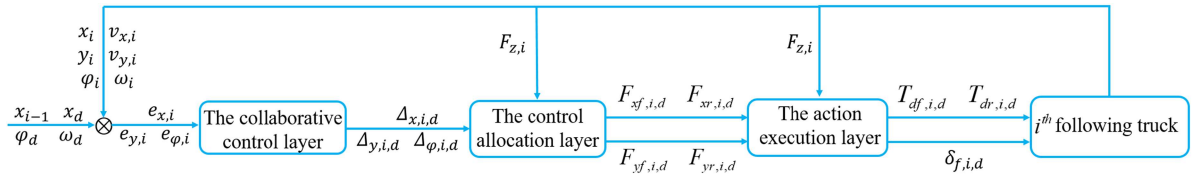

Figure 3. The structure with longitudinal and lateral coupling control.

drive torque and the expected front wheel angle. The proposed control scheme is shown in Figure 3, which can effectively ensure safe travelling of the platoon.

3.1 The cooperative control layer

In this section, a distributed sliding mode controller based on finite-time reachability is designed for the platoon model (Liu 2012; Sundarapandian and Lien 2017), using the error $E(t)$ of the ith following truck as the basis for the design.

Firstly, the coupled sliding mode switching function is defined as follows:

$$\begin{cases} s_{x,i}^{c}(t) = \dot{e}_{x,i}(t) + c_1 e_{x,i}(t) + c_2 e_{x,i}^{p}(t) \\ s_{y,i}^{c}(t) = \dot{e}_{y,i}(t) + c_3 e_{y,i}(t) + c_4 e_{y,i}^{q}(t) \\ s_{\varphi,i}^{c}(t) = \dot{e}_{\varphi,i}(t) + c_5 e_{\varphi,i}(t) + c_6 e_{\varphi,i}^{r}(t) \end{cases}, \tag{21}$$

where p, q, and r represent ratios of two positive odd numbers, while terms of c_1 to c_6 represent positive parameters.

Note that in the sliding surfaces defined in Equation (21), the parameters p, q, and r are design parameters chosen as ratios of two positive odd integers. This specific choice is fundamental to the design of the terminal sliding mode surface, as it guarantees that the system states converge to the equilibrium in finite time and avoids singularity issues in the control law (Gambhire et al. 2021).

By taking the derivative of Equation (21):

$$\begin{cases} \dot{s}_{x,i}^{c}(t) = \ddot{e}_{x,i}(t) + c_1 \dot{e}_{x,i}(t) + c_2 p e_{x,i}^{p-1}(t) \dot{e}_{x,i}(t) \\ \dot{s}_{y,i}^{c}(t) = \ddot{e}_{y,i}(t) + c_3 \dot{e}_{y,i}(t) + c_4 q e_{y,i}^{q-1}(t) \dot{e}_{y,i}(t), \\ \dot{s}_{\varphi,i}^{c}(t) = \ddot{e}_{\varphi,i}(t) + c_5 \dot{e}_{\varphi,i}(t) + c_6 r e_{\varphi,i}^{r-1}(t) \dot{e}_{\varphi,i}(t) \end{cases} \tag{22}$$

The coupled exponential convergence law is chosen:

$$\begin{cases} \dot{s}_{x,i}^{c}(t) = -k_1 s_{x,i}^{c}(t) - \eta_1 \operatorname{sgn}\left(s_{x,i}^{c}(t)\right) \\ \qquad\qquad - D_{x,i}(t) \operatorname{sgn}\left(s_{x,i}^{c}(t)\right) \\ \dot{s}_{y,i}^{c}(t) = -k_2 s_{y,i}^{c}(t) - \eta_2 \operatorname{sgn}\left(s_{y,i}^{c}(t)\right) \\ \qquad\qquad - D_{y,i}(t) \operatorname{sgn}\left(s_{y,i}^{c}(t)\right) \\ \dot{s}_{\varphi,i}^{c}(t) = -k_3 s_{\varphi,i}^{c}(t) - \eta_3 \operatorname{sgn}\left(s_{\varphi,i}^{c}(t)\right) \\ \qquad\qquad - D_{\varphi,i}(t) \operatorname{sgn}\left(s_{\varphi,i}^{c}(t)\right) \end{cases}, \tag{23}$$

where k_1, k_2, k_3, η_1, η_2 and η_3 represent positive parameters. Define $D_i(t) = [D_{x,i}(t), D_{y,i}(t), D_{\varphi,i}(t)]^T$ as an upper bound on the unknown perturbations present in the system. By taking the second-order derivative of $E(t)$, and it can be described as:

$$\begin{cases} \ddot{e}_{x,i}(t) = & \dot{v}_{x,i}(t) - \sigma_1 \dot{v}_{x,0}(t) - \sigma_2 \dot{v}_{x,i-1}(t) + d_{x,i}(t) \\ \ddot{e}_{y,i}(t) = & v_{x,i}(t)[\omega_{d,i}(t) - \omega_i(t)] - \dot{v}_{y,i}(t) \\ & - L_y \dot{\omega}_i(t) + d_{y,i}(t) \\ \ddot{e}_{\varphi,i}(t) = & - \dot{\omega}_i(t) + d_{\varphi,i}(t) \end{cases}, \tag{24}$$

where it satisfies $|d_{x,i}(t)| \le D_{x,i}(t)$, $|d_{y,i}(t)| \le D_{y,i}(t)$ and $|d_{\varphi,i}(t)| \le D_{\varphi,i}(t)$. The terms $\dot{v}_{x,i}(t)$, $\dot{v}_{x,i-1}(t)$ and $\dot{v}_{x,0}(t)$ represent the longitudinal speed of the ith following truck, the longitudinal speed of the $(i-1)$th following truck and the longitudinal speed of the leading truck, respectively. The term $\dot{\omega}_i(t)$ is the yaw angle acceleration rate of the ith following truck.

By combining Equations (15) and (24), the system can be described as three subsystems with unknown upper bound perturbations:

$$\begin{cases} \dot{e}_{x,i}(t) &= v_{x,i}(t) - \sigma_1 v_{x,0}(t) - \sigma_2 v_{x,i-1}(t) \\ \ddot{e}_{x,i}(t) &= \dot{v}_{x,i}(t) - \sigma_1 \dot{v}_{x,0}(t) - \sigma_2 \dot{v}_{x,i-1}(t) + d_{x,i}(t) \end{cases}$$
$$\begin{cases} \dot{e}_{y,i}(t) &= v_{x,i}(t) e_{\varphi,i}(t) - v_{y,i}(t) - L_y \omega_i(t) \\ \ddot{e}_{y,i}(t) &= v_{x,i}(t)[\omega_{d,i}(t) - \omega_i(t)] - \dot{v}_{y,i}(t) \\ & -L_y \dot{\omega}_i(t) + d_{y,i}(t) \end{cases}. \tag{25}$$
$$\begin{cases} \dot{e}_{\varphi,i}(t) &= \omega_{d,i}(t) - \omega_i(t) \\ \ddot{e}_{\varphi,i}(t) &= -\dot{\omega}_i(t) + d_{\varphi,i}(t) \end{cases}$$

Therefore, the coupling control law for the ith following truck is derived, where the desired longitudinal acceleration, lateral acceleration, and yaw angle acceleration rates of the ith following truck are:

$$\begin{cases} \dot{v}_{x,i,d}(t) &= \sigma_1 \dot{v}_{x,0}(t) + \sigma_2 \dot{v}_{x,i-1}(t) - Q_{x,i}(t) \\ \dot{v}_{y,i,d}(t) &= v_{x,i}(t)[\omega_{d,i}(t) - \omega_i(t)] - L_y \dot{\omega}_i(t) + Q_{y,i}(t), \\ \dot{\omega}_{i,d}(t) &= Q_{\varphi,i}(t) \end{cases} \tag{26}$$

where,

$$\begin{cases} Q_{x,i}(t) &= c_1 \dot{e}_{x,i}(t) + c_2 p e_{x,i}^{p-1}(t) \dot{e}_{x,i}(t) + k_1 s_{x,i}^c(t) \\ & \quad + \eta_1 \operatorname{sgn}\left(s_{x,i}^c(t)\right) + D_{x,i}(t) \operatorname{sgn}\left(s_{x,i}^c(t)\right) \\ Q_{y,i}(t) &= c_3 \dot{e}_{y,i}(t) + c_4 q e_{y,i}^{q-1}(t) \dot{e}_{y,i}(t) + k_2 s_{y,i}^c(t) \\ & \quad + \eta_2 \operatorname{sgn}\left(s_{y,i}^c(t)\right) + D_{y,i}(t) \operatorname{sgn}\left(s_{y,i}^c(t)\right), \\ Q_{\varphi,i}(t) &= c_5 \dot{e}_{\varphi,i}(t) + c_6 r e_{\varphi,i}^{r-1}(t) \dot{e}_{\varphi,i}(t) + k_3 s_{\varphi,i}^c(t) \\ & \quad + \eta_3 \operatorname{sgn}\left(s_{\varphi,i}^c(t)\right) + D_{\varphi,i}(t) \operatorname{sgn}\left(s_{\varphi,i}^c(t)\right) \end{cases} \tag{27}$$

Therefore, the required control input for the ith following truck in the platoon can be determined as follows:

$$\begin{cases} \Delta_{x,i,d}(t) &= F_{wx,i}(t) - m_i v_{y,i}(t) \omega_i(t) + m_i \sigma_1 \dot{v}_{x,0}(t) \\ & \quad + m_i \sigma_2 \dot{v}_{x,i-1}(t) - m_i Q_{x,i}(t) \\ \Delta_{y,i,d}(t) &= F_{wy,i}(t) + m_i K v_{x,i}^2(t) + m_i Q_{y,i}(t) \\ & \quad - m_i L_{y,i} Q_{\varphi,i}(t) \\ \Delta_{\varphi,i,d}(t) &= I_{z,i} Q_{\varphi,i}(t) \end{cases}, \tag{28}$$

and Equation (28) can be expressed in matrix form as follows:

$$\begin{bmatrix} \Delta_{x,i,d}(t) \\ \Delta_{y,i,d}(t) \\ \Delta_{\varphi,i,d}(t) \end{bmatrix} = \begin{bmatrix} m_i & 0 & 0 \\ 0 & m_i & -m_i L_y \\ 0 & 0 & I_{z,i} \end{bmatrix} \begin{bmatrix} \lambda_{x,i}(t) \\ \lambda_{y,i}(t) \\ \lambda_{\varphi,i}(t) \end{bmatrix}, \tag{29}$$

where $\lambda_i(t) = [\lambda_{x,i}(t), \lambda_{y,i}(t), \lambda_{\varphi,i}(t)]^T$.

Define $\Delta_{i,d}(t) = \Phi_i \lambda_i(t)$, where $\lambda_i(t)$ and Φ_i can be defined respectively as:

$$\begin{cases} \lambda_{x,i}(t) &= \frac{1}{m_i} F_{wx,i}(t) - [v_{y,i}(t)\omega_i(t) - \sigma_1 \dot{v}_{x,0}(t) \\ & \quad -\sigma_2 \dot{v}_{x,i-1}(t) + Q_{x,i}(t)] \\ \lambda_{y,i}(t) &= \frac{1}{m_i} F_{wy,i}(t) + K v_{x,i}^2(t) + Q_{y,i}(t) \\ \lambda_{\varphi,i}(t) &= Q_{\varphi,i}(t) \end{cases}, \tag{30}$$

$$\Phi_i = \begin{bmatrix} m_i & 0 & 0 \\ 0 & m_i & -m_i L_y \\ 0 & 0 & I_{z,i} \end{bmatrix}. \tag{31}$$

where $|\Phi_i| = I_{z,i} m_i^2 \neq 0$, and it indicates that Φ_i is a non-singular matrix. In the cooperative control layer, a non-singular control law is established of the ith following truck in the platoon, defined as $\Delta_{i,d}(t) = \Phi_i \lambda_i(t)$.

3.2 The control allocation layer

The desired tire forces for the ith following truck in the platoon, $\Delta_i(t)$, obtained from the cooperative control layer, will be optimally allocated by the control allocation layer into the front and rear longitudinal tire forces, as well as the front and rear lateral tire forces.

The objective of the control allocation layer is to calculate the optimal desired tire forces for the ith following truck, denoted as $F_{i,d}(t) = [F_{xf,i,d}(t), F_{yf,i,d}(t), F_{xr,i,d}(t), F_{yr,i,d}(t)]^T$, in order to approximate $\Delta_{i,d}(t)$. The desired control input for the ith following truck is defined as:

$$\begin{cases} \Delta_{x,i,d}(t) = F_{xf,i,d}(t) + F_{xr,i,d}(t) \\ \Delta_{y,i,d}(t) = F_{yf,i,d}(t) + F_{yr,i,d}(t) \\ \Delta_{\varphi,i,d}(t) = aF_{yf,i,d}(t) - bF_{yr,i,d}(t) \end{cases}. \tag{32}$$

The term of Equation (32) can be rewritten as:

$$\Delta_{i,d}(t) = M_{f,i} F_{i,d}(t), \tag{33}$$

where the matrix $M_{f,i}$ is shown as:

$$M_{f,i} = \begin{bmatrix} 1 & 0 & 1 & 0 \\ 0 & 1 & 0 & 1 \\ 0 & a & 0 & -b \end{bmatrix}. \tag{34}$$

In order to minimise both the error and energy consumption, based on the principle of power minimisation and subject to constraints on the lateral and longitudinal tire forces of the truck, the optimisation problem in the control allocation layer can be formulated as follows:

$$\begin{aligned} &\min J(F_{i,d}) \\ &s.t. \end{aligned}, \tag{35a}$$

$$F_{xf,i,\min} \leq F_{xf,i,d} \leq F_{xf,i,\max}, \tag{35b}$$

$$F_{yf,i,\min} \leq F_{yf,i,d} \leq F_{yf,i,\max}, \tag{35c}$$

$$F_{xr,i,\min} \le F_{xr,i,d} \le F_{xr,i,\max}, \tag{35d}$$

$$F_{yr,i,\min} \le F_{yr,i,d} \le F_{yr,i,\max}, \tag{35e}$$

$$\sqrt{F_{xf,i,d}^2 + F_{yf,i,d}^2} \le \mu F_{zf,i}, \tag{35f}$$

$$\sqrt{F_{xr,i,d}^2 + F_{yr,i,d}^2} \le \mu F_{zr,i}, \tag{35g}$$

where,

$$\begin{aligned} J(F_{i,d}) \;=\; & \tfrac{1}{2}(\Delta_{i,d} - M_{f,i}F_{i,d})^T Q\,(\Delta_{i,d} - M_{f,i}F_{i,d}) \\ & + \tfrac{1}{2}F_{i,d}{}^T R F_{i,d} \end{aligned}, \tag{36}$$

and the terms of $F_{zf,i}$ and $F_{zr,i}$ represent the vertical loads on the front and rear wheels of the ith following truck, respectively, and Q and R are positive definite symmetric weighting matrices.

Remark 4. The positive definite symmetric weighting matrices Q and R are design parameters that balance the trade-off between the tracking accuracy of the generalised forces and the magnitude of the tire forces. In this work, after preliminary tuning, these matrices are selected as $Q = \mathrm{diag}(1, 1, 1)$ and $R = \mathrm{diag}(1, 1, 1, 1)$. The choice of identity matrices as a baseline is found to provide robust and satisfactory performance, effectively meeting the control objectives for both longitudinal tracking and lateral stability without requiring further fine-tuning. Future work will include a systematic sensitivity analysis and potentially an automatic tuning procedure for the weighting matrices in the control allocation layer to further optimise performance and provide generalisable design guidelines.

The objective function is convex, ensuring a globally optimal solution. It is important to consider both the error and control input consumption when selecting weighting matrices. The resulting constrained optimisation problem is solved using a standard nonlinear programming approach that is based on an interior-point method. The associated computational performance and real-time feasibility are summarised in Table 2.

3.3 The action execution layer

In the control allocation layer, the expected tire forces for the ith following truck are calculated. To convert $F_{i,d}$ into the final control inputs: front and rear wheel drive torques and the front wheel steering angle, this section constructs an action execution layer consisting of a tire model and torque formula. Among them, the 'magic formula tire model is used to invert the expected lateral force of the front tire into the desired front wheel slip angle, while the torque formula can directly calculate the expected longitudinal force of the front and rear wheels to obtain the desired front and rear wheel driving torques. Once the desired tire force is obtained by the control allocation layer, the action execution layer will be activated.

From the 'magic formula', the desired front wheel lateral force $F_{yf,i,d}(t)$ of the ith following truck corresponds to the desired front wheel slip angle $\alpha_{f,i,d}(t)$. The specific relationship can be expressed as follows:

$$\alpha_{f,i,d}(t) = \Pi^{-1}(F_{yf,i,d}(t)), \tag{37}$$

where Π^{-1} represents the inverse of the 'magic formula' tire model, which is approximated using a least squares algorithm to determine the desired front wheel slip angle.

Table 2. The values of computation time.

Optimisation method	Max time	Min time	Average time	Sample time
Interior-point method	0.15 ms	0.06 ms	0.1 ms	10 ms

Remark 5. The inversion of the 'magic formula' to obtain the desired slip angle from the desired lateral force is implemented using a numerical root-finding approach. In this study, MATLAB's fsolve solver is utilised, which employs a trust-region-dogleg algorithm. This algorithm is structurally based on the Gauss–Newton method, a foundational technique for nonlinear least-squares problems. Therefore, the reference to 'a least squares algorithm' pertains to the underlying mathematical principle of the solver used to find the root of the equation and not to a sequential online parameter fitting routine. For embedded deployment, this step can be implemented with a lightweight, fixed-point Newton–Raphson or secant method solver, maintaining the core numerical approach without reliance on MATLAB's computational environment.

Figure 4 illustrates the relationship between the lateral force exerted by the tire and the slip angle under varying vertical loads. It can be observed that when the desired lateral force of the tire is low, the desired slip angle is also relatively small. However, as the desired lateral force of the tire increases, it corresponds to two desired slip angles: one in the linear region and the other in the nonlinear region of the curve.

As shown in Figure 5, the constraints on the tire forces can be categorised into linear and nonlinear zone constraints. It is essential to select the appropriate slip angle based on these different constraints (Guo, Li, and Luo 2015).

Once the control allocation layer determines the desired longitudinal and lateral front tire forces based on the objective function, it becomes essential to assess whether the tire force constraints are met. This assessment is necessary when the longitudinal and lateral tire forces satisfy the following condition:

$$0 \le \sqrt{F_{xf,i,d}^2 + F_{yf,i,d}^2} \le \frac{1}{2}\mu F_{zf,i} b. \tag{38}$$

In this case, the desired front wheel slip angle, $\alpha_{f,i,d}(t)$, should be selected within the linear zone. Similarly, when the longitudinal and lateral tire force constraints satisfy the following condition:

$$\frac{1}{2}\mu F_{zf,i} \le \sqrt{F_{xf,i,d}^2 + F_{yf,i,d}^2} \le \mu F_{zf,i}. \tag{39}$$

Then, the expected front wheel slip angle, $\alpha_{f,i,d}(t)$, should be selected within the nonlinear zone.

Therefore, the desired front wheel steering angle, $\delta_{f,i,d}$, for the ith following truck can be determined as follows:

$$\delta_{f,i,d}(t) = \alpha_{f,i,d}(t) + \arctan\left(\frac{v_{y,i}(t) + a\omega_i(t)}{v_{x,i}(t)}\right). \tag{40}$$

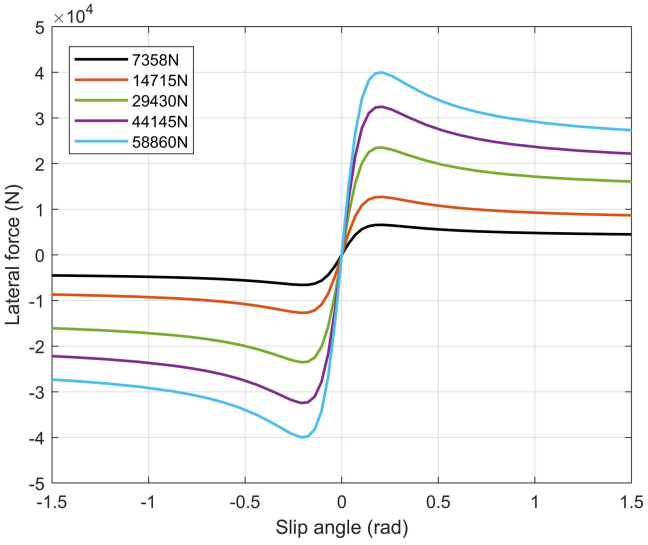

Figure 4. Diagram of the relationship between tire lateral force and slip angle.

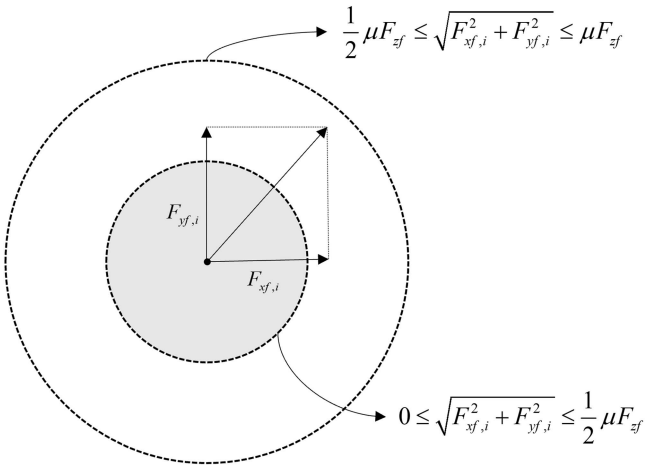

Figure 5. Tire force constraint diagram.

Similarly, the longitudinal control input for the *i*th following truck can be calculated using the torque equation, which is based on the desired longitudinal front tire force $F_{xf,i,d}(t)$ and the desired longitudinal rear tire force $F_{xr,i,d}(t)$ obtained from the control allocation layer. The desired front wheel drive torque $T_{df,i,d}(t)$ and desired rear wheel drive torque $T_{dr,i,d}(t)$ are expressed as follows:

$$\begin{cases} T_{df,i,d}(t) = RF_{xf,i,d}(t) \\ T_{dr,i,d}(t) = RF_{xr,i,d}(t)' \end{cases} \tag{41}$$

Remark 6. The front and rear driving torques obtained in this paper represent the expected driving torques for the following trucks. However, owing to mechanical efficiency losses in the torque transmission of trucks, the calculated driving torques may deviate from the actual value and cannot be directly applied to the throttle valves (Zhang et al. 2021). Therefore, the actual control input acting on the throttle valves should be determined based on the trucks' engine model.

Remark 7. The classification of the tire operating condition into linear and nonlinear zones via Equations (38) and (39) serves a practical and essential purpose in real-time control. Rather than aiming to guarantee the global mathematical uniqueness of the inverse magic-formula mapping, this zonal strategy ensures that the selected slip-angle lies within a physically meaningful and feasible operating range of the tire. By restricting the inversion to the monotonic linear region or the admissible saturation nonlinear region, the controller naturally avoids multi-valued or non-physical branches of the full 'Magic-Formula' curve. This guarantees that, for any feasible desired tire-force vector within the friction circle, a single physically realisable slip-angle can be selected for execution-meeting the core requirement for safety-critical real-time applications.

3.4 Properties of truck platoons

In this section, the properties of truck platoons, i.e. finite-time reachability and string stability, are investigated.

Lemma 3.1. (Yanjun and Huang 2009) Consider the autonomous system,

$$\Xi = \Gamma(\Xi), \quad \Xi(0) = \Xi_0, \tag{42}$$

where $\Gamma \in \mathbb{R}^n \to \mathbb{R}^n$ is continuous on an open neighbourhood of the origin $\Xi = 0$, and $\Gamma(0) = 0$.

Suppose that there exists a continuous differentiable function $\mathfrak{I}: \mathbb{R}^n \to \mathbb{R}^n$, scalars $\tilde{\lambda}$, $\tilde{\gamma} > 0$, $\tilde{\beta} \in (0,1)$, and an open neighbourhood $\tilde{M}$ of the origin such that,

$$\dot{\mathfrak{I}}(\Xi) \leq -\tilde{\gamma}\mathfrak{I}(\Xi) - \tilde{\lambda}\mathfrak{I}(\Xi)^{\tilde{\beta}}. \tag{43}$$

For all $\Xi \in \tilde{M} \setminus \{0\}$, $\mathfrak{I}(\Xi) > 0$, and $\mathfrak{I}(0) = 0$. The origin of the system Equation (42) is finite-time reachable, and the setting time T_s satisfies (Liu et al. 2022):

$$T_s \leq \frac{1}{\tilde{\gamma}(1-\tilde{\beta})} \ln\left(1 + \frac{\tilde{\gamma}}{\tilde{\lambda}}\mathfrak{I}(\Xi_0)^{1-\tilde{\beta}}\right). \tag{44}$$

Theorem 1. The state of system Equation (25) can reach the sliding mode surface Equation (21) in finite time.

Proof 1. Define a candidate Lyapunov function for *i*th following truck:

$$V_i(t) = \frac{1}{2}\left(s_{x,i}^c(t)\right)^2 + \frac{1}{2}\left(s_{y,i}^c(t)\right)^2 + \frac{1}{2}\left(s_{\varphi,i}^c(t)\right)^2 c. \tag{45}$$

By taking the derivative of Equation (45), one has:

$$\dot{V}_i(t) = s_{x,i}^c(t)\dot{s}_{x,i}^c(t) + s_{y,i}^c(t)\dot{s}_{y,i}^c(t) + s_{\varphi,i}^c(t)\dot{s}_{\varphi,i}^c(t). \tag{46}$$

Combining Equations (22), (24) and Equation (46), one has:

$$\begin{aligned}
\dot{V}_i(t) \;=\; & s_{x,i}^c(t)(\dot{v}_{x,i}(t) - \sigma_1\dot{v}_{x,0}(t) - \sigma_2\dot{v}_{x,i-1}(t)) \\
& + s_{x,i}^c(t)(c_1\dot{e}_{x,i}(t) + c_2 p e_{x,i}^{p-1}(t)\dot{e}_{x,i}(t) + d_{x,i}(t)) \\
& + s_{y,i}^c(t)(v_{x,i}(t)[\omega_{d,i}(t) - \omega_i(t)]) \\
& + s_{y,i}^c(t)(-\dot{v}_{y,i}(t) - L_y\dot{\omega}_i(t)) \\
& + s_{y,i}^c(t)(c_3\dot{e}_{y,i}(t) + c_4 q e_{y,i}^{q-1}(t)\dot{e}_{y,i}(t) + d_{y,i}(t)) \\
& + s_{\varphi,i}^c(t)(-\dot{\omega}_i(t) + c_5\dot{e}_{\varphi,i}(t)) \\
& + s_{\varphi,i}^c(t)(c_6 r e_{\varphi,i}^{r-1}(t)\dot{e}_{\varphi,i}(t) + d_{\varphi,i}(t))
\end{aligned} \tag{47}$$

Combining Equations (26), (27) and Equation (47), one has:

$$\begin{aligned}
\dot{V}_i(t) = \; & s_{x,i}^c(t)\left(-k_1 s_{x,i}^c(t) - \eta_1 \operatorname{sgn}\left(s_{x,i}^c(t)\right)\right) \\
& + s_{x,i}^c(t)\left(d_{x,i}(t) - D_{x,i}(t)\operatorname{sgn}\left(s_{x,i}^c(t)\right)\right) \\
& + s_{y,i}^c(t)\left(-k_2 s_{y,i}^c(t) - \eta_2 \operatorname{sgn}\left(s_{y,i}^c(t)\right)\right) \\
& + s_{y,i}^c(t)\left(d_{y,i}(t) - D_{y,i}(t)\operatorname{sgn}\left(s_{y,i}^c(t)\right)\right) \\
& + s_{\varphi,i}^c(t)\left(-k_3 s_{\varphi,i}^c(t) - \eta_3 \operatorname{sgn}\left(s_{\varphi,i}^c(t)\right)\right) \\
& + s_{\varphi,i}^c(t)\left(d_{\varphi,t}(t) - D_{\varphi,i}(t)\operatorname{sgn}\left(s_{\varphi,i}^c(t)\right)\right)
\end{aligned} \tag{48}$$

Then, Equation (48) can be rewritten as:

$$\begin{aligned}\dot{V}_i(t) = & -k_1\left(s_{x,i}^c(t)\right)^2 - \eta_1\left|s_{x,i}^c(t)\right| \\ & + d_{x,i}(t)s_{x,i}^c(t) - D_{x,i}(t)\left|s_{x,i}^c(t)\right| \\ & - k_2\left(s_{y,i}^c(t)\right)^2 - \eta_2\left|s_{y,i}^c(t)\right| \\ & + d_{y,i}(t)s_{y,i}^c(t) - D_{y,i}(t)\left|s_{y,i}^c(t)\right| \\ & - k_3\left(s_{\varphi,i}^c(t)\right)^2 - \eta_3\left|s_{\varphi,i}^c(t)\right| \\ & + d_{\varphi,i}(t)s_{\varphi,i}^c(t) - D_{\varphi,i}(t)\left|s_{\varphi,i}^c(t)\right|\end{aligned}. \tag{49}$$

According to Equation (49), one has:

$$\begin{aligned}\dot{V}_i(t) \leq & -k_1\left(s_{x,i}^c(t)\right)^2 - \eta_1\left|s_{x,i}^c(t)\right| \\ & + |d_{x,i}(t)|\left|s_{x,i}^c(t)\right| - D_{x,i}(t)\left|s_{x,i}^c(t)\right| \\ & - k_2\left(s_{y,i}^c(t)\right)^2 - \eta_2\left|s_{y,i}^c(t)\right| \\ & + |d_{y,i}(t)|\left|s_{y,i}^c(t)\right| - D_{y,i}(t)\left|s_{y,i}^c(t)\right| \\ & - k_3\left(s_{\varphi,i}^c(t)\right)^2 - \eta_3\left|s_{\varphi,i}^c(t)\right| \\ & + |d_{\varphi,i}(t)|\left|s_{\varphi,i}^c(t)\right| - D_{\varphi,i}(t)\left|s_{\varphi,i}^c(t)\right| \\ \leq & -k_1\left(s_{x,i}^c(t)\right)^2 - k_2\left(s_{y,i}^c(t)\right)^2 - k_3\left(s_{\varphi,i}^c(t)\right)^2 \\ & - \eta_1\left|s_{x,i}^c(t)\right| - \eta_2\left|s_{y,i}^c(t)\right| - \eta_3\left|s_{\varphi,i}^c(t)\right|\end{aligned}. \tag{50}$$

According to Equation (45), one has:

$$\begin{cases} 2V_i(t) = \left(s_{x,i}^c(t)\right)^2 + \left(s_{y,i}^c(t)\right)^2 + \left(s_{\varphi,i}^c(t)\right)^2 \\ \sqrt{2V_i(t)} = \sqrt{\left(s_{x,i}^c(t)\right)^2 + \left(s_{y,i}^c(t)\right)^2 + \left(s_{\varphi,i}^c(t)\right)^2} \end{cases}. \tag{51}$$

Combining Equations (50) and (51), one has:

$$\begin{aligned}\dot{V}_i(t) &\le -k_1\left(s^c_{x,i}(t)\right)^2 - k_2\left(s^c_{y,i}(t)\right)^2 - k_3\left(s^c_{\varphi,i}(t)\right)^2 \\ &\quad -\eta_1\left|s^c_{x,i}(t)\right| - \eta_2\left|s^c_{y,i}(t)\right| - \eta_3\left|s^c_{\varphi,i}(t)\right| \\ &\le -\tfrac{2(k_1+k_2+k_3)}{3}V_i(t) \\ &\quad -\tfrac{\sqrt{2}(\eta_1+\eta_2+\eta_3)}{3}(V_i(t))^{0.5}\end{aligned} \tag{52}$$

Therefore, it satisfies $V_i(t) > 0$ and $\dot{V}_i(t) < 0$. According to Lemma 3.1, the system states can reach the sliding mode surface in finite time, and the setting time t_r^c satisfies:

$$t_r^c \le \frac{3}{k_1+k_2+k_3}\ln\left(1+\frac{\sqrt{2}(k_1+k_2+k_3)}{\eta_1+\eta_2+\eta_3}V_i(0)^{0.5}\right). \tag{53}$$

Remark 8. The finite-time stability proof of the proposed sliding mode controller relies on the standard theoretical assumption that the upper bounds of the disturbances are known (Liu, Yue, et al. 2025; Zuo et al. 2025). In practice, these bounds can be estimated conservatively based on the worst-case operational scenarios. It is important to note that the primary focus of this paper is to establish the performance baseline of the coupled control framework. The integration of disturbance observers or adaptive techniques to obviate the need for a priori bound knowledge is a key objective for future research aimed at enhancing practical robustness.

Theorem 2. The spacing errors are not amplified along the platoon, i.e. the truck platoon is string stable in steady state.

Proof 2. When a truck platoon is in steady state, $e_{x,i}(t) = 0$ and $e_{x,i-1}(t) = 0$, according to Equation (12), one has:

$$\begin{cases}\sigma_1 e_{i,0}(t) + \sigma_2 e_i(t) = 0 \\ \sigma_1 e_{i-1,0}(t) + \sigma_2 e_{i-1}(t) = 0'\end{cases} \tag{54}$$

where σ_1 and σ_2 are positive parameters, and $\sigma_1 + \sigma_2 = 1$.

In terms of Equation (11), one has:

$$\begin{cases}e_{i,0}(t) = e_1(t) + e_2(t) + e_3(t)\ldots + e_i(t) \\ e_{i-1,0}(t) = e_1(t) + e_2(t) + e_3(t)\ldots + e_{i-1}(t)\end{cases}. \tag{55}$$

In terms of Equations (54) and (55), one has:

$$\begin{cases}e_1(t) + e_2(t) + e_3(t)\ldots + e_{i-1}(t) + \left(1+\frac{\sigma_2}{\sigma_1}\right)e_i(t) = 0 \\ e_{i-1,0}(t) + \frac{\sigma_2}{\sigma_1}e_{i-1}(t) = 0\end{cases}. \tag{56}$$

By simplification of Equation (56), one has:

$$\left(1+\frac{\sigma_2}{\sigma_1}\right)e_i(t) = \frac{\sigma_2}{\sigma_1}e_{i-1}(t). \tag{57}$$

Applying the Laplace transform to Equation (57), one has:

$$\left\| \frac{e_i(s)}{e_{i-1}(s)} \right\| = \left\| \frac{\sigma_2}{\sigma_1}\cdot\frac{\sigma_1}{\sigma_1+\sigma_2} \right\| = \sigma_2. \tag{58}$$

Since $\sigma_1 > 0$, $\sigma_2 > 0$, $\sigma_1 + \sigma_2 = 1$ and $0 < \sigma_2 < 1$, according to Equation (18), the truck platoon is string stable.

Note that, on the one hand, steady-state string stability guarantees that the cooperative control structure does not intrinsically amplify spacing errors along the platoon (Xiao and Gao 2011; Zhu et al. 2024). On the other hand, the proposed sliding-mode controller drives tracking errors to the sliding surface within a finite time during the transient phase, even in the presence of uncertainties and model–plant mismatches, such as unmodeled actuator dynamics. As a result, after finite-time convergence, the closed-loop system operates in the steady state, where the string stability conditions are satisfied and spacing errors do not amplify along the platoon. A more comprehensive theoretical treatment that explicitly incorporates actuator dynamics will be an important direction for future work.

Remark 9. Theorem 2 establishes the steady-state string stability of the platoon under the constant-spacing policy, following the classical frequency-domain definition in Equation (18). This analysis focuses on equilibrium properties and asymptotic error propagation. Transient robustness to disturbances is ensured by the finite-time convergent sliding-mode dynamics established in Theorem 1. The analysis of communication delays and their impact on string stability is beyond the current scope and will be investigated in future work.

4 Simulation experiments and analysis

In this section, a truck platoon consisting of a leading truck and four following trucks is selected for the simulation using the joint platform of TruckSim and Simulink. The system states are the longitudinal velocity, lateral velocity, yaw angle rate, and angular velocities of the front and rear wheels. The control inputs are the driving torque and front wheel steering angle of the trucks. The parameters of the trucks, tires, and controllers are listed in Tables 3–5, respectively.

In this paper, given that the width of a typical highway lane is approximately 3.5 m, and the width of a truck is about 2.5 m, the permissible constraint on the lateral error is ±0.5 m. This constraint complies with the lateral control standards outlined in the test protocol for autonomous driving functions in intelligent networked vehicles (Ding et al. 2023).

In practical implementation of the controller, to mitigate the chattering phenomenon and generate smooth control commands feasible for vehicle actuators, the sgn(s) function is replaced by the continuous saturation function sat(s/Δ), defined as:

$$\text{sat}\,(s/\Delta) = \begin{cases} \text{sgn}\,(s), & |s| > \Delta \\ s/\Delta, & |s| \le \Delta \end{cases}, \tag{59}$$

where $\Delta > 0$ is the boundary layer thickness, which is a design parameter tuned to suppress chattering while maintaining acceptable tracking performance. In this study, the value of Δ is selected as 0.5.

Table 3. The parameters of trucks.

Parameters	Value	Parameters	Value
m	18,000 kg	I_z	130421.8 kg m^2
a	3.5 m	b	1.5 m
C_x	0.6	C_y	0.8
A_x	6.8 m^2	A_y	11.25 m^2
J_f	24 kg m^2	J_r	48 kg m^2
r	0.51 m	ρ	1.2258 kg/m^3

Table 4. The parameters of tires.

Tire forces	B	C	D	E
F_{xf0}	8.61	1.58	22503	0.5624
F_{xr0}	8.61	1.58	44625	0.5624
F_{yf0}	6.59	1.58	22503	−0.3028
F_{yr0}	6.59	1.58	44625	−0.3028

Table 5. The parameters of controllers.

Parameters	Value	Parameters	Value
c_1	1	k_1	1
c_2	1	k_2	5
c_3	1	k_3	2
c_4	0.1	η_1	0.1
c_5	5	η_2	0.1
c_6	1	η_3	0.1
σ_1	0.4	p	3/5
σ_2	0.6	q	3/5
Q	diag (1, 1, 1)	r	3/5
R	diag (1, 1, 1, 1)	$r_{x,1}$	35
$r_{x,2}$	40	$r_{y,1}$	40
$r_{y,2}$	35		

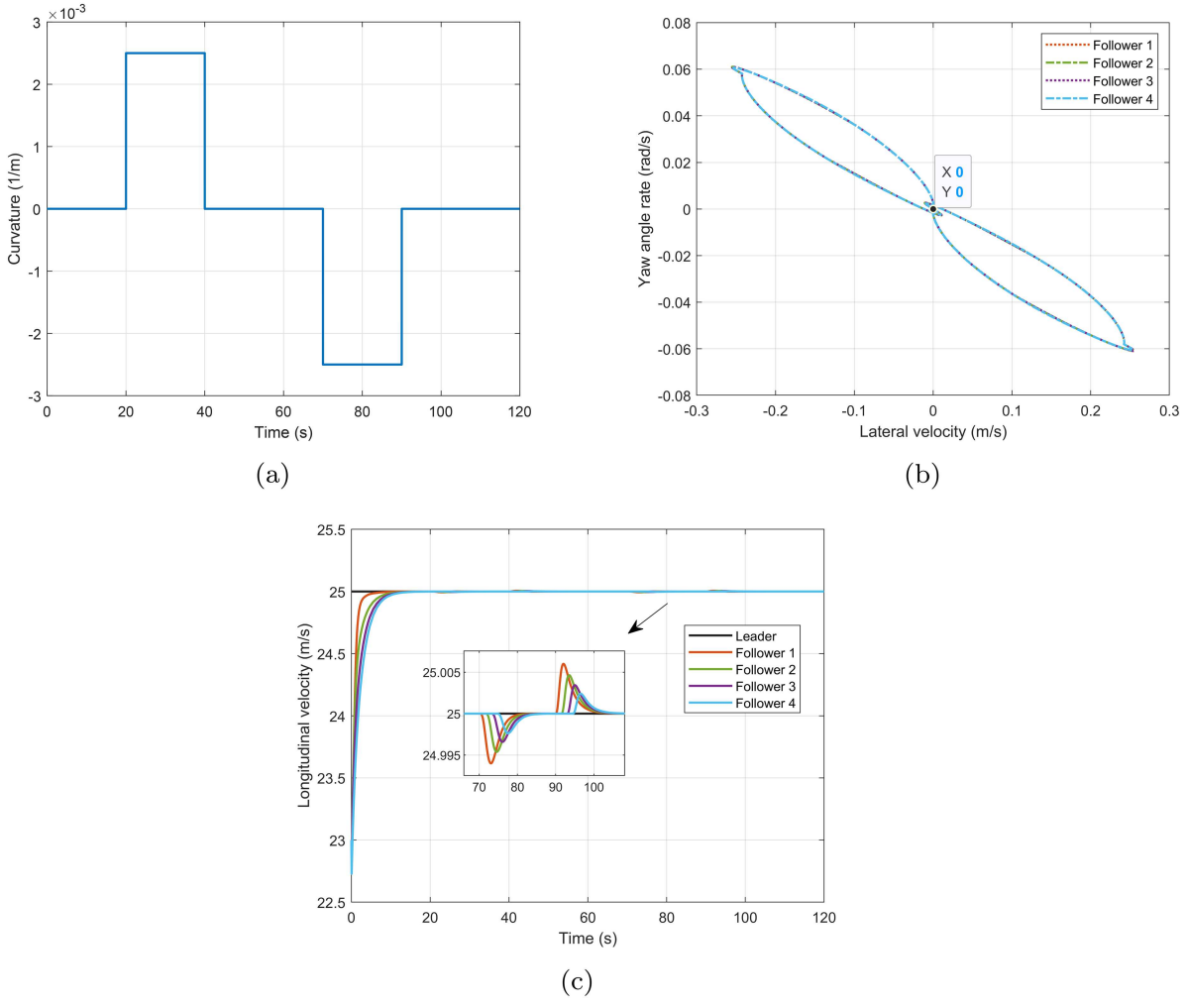

Figure 6. Truck platoon in scenario 1: (a) road curvature, (b) phase trajectories, and (c) longitudinal velocities.

4.1 Scenario 1: high-speed

In order to verify the effectiveness of the proposed hierarchical control scheme for truck platoons driving on a motorway, the maximum road curvature of 0.0025 and the road surface adhesion coefficient of 0.85 are selected (Sun et al. 2023; Zhao et al. 2023). The leading truck is set to travel at a constant speed of 25 m/s, the initial speed of the following trucks is 23 m/s, and the initial longitudinal spacing errors between the leading truck and the four following trucks are set as 2, 3, 4, and 5 m, respectively. The initial lateral position errors and yaw angle errors of the trucks are 0. The simulation results are shown in Figures 6–8.

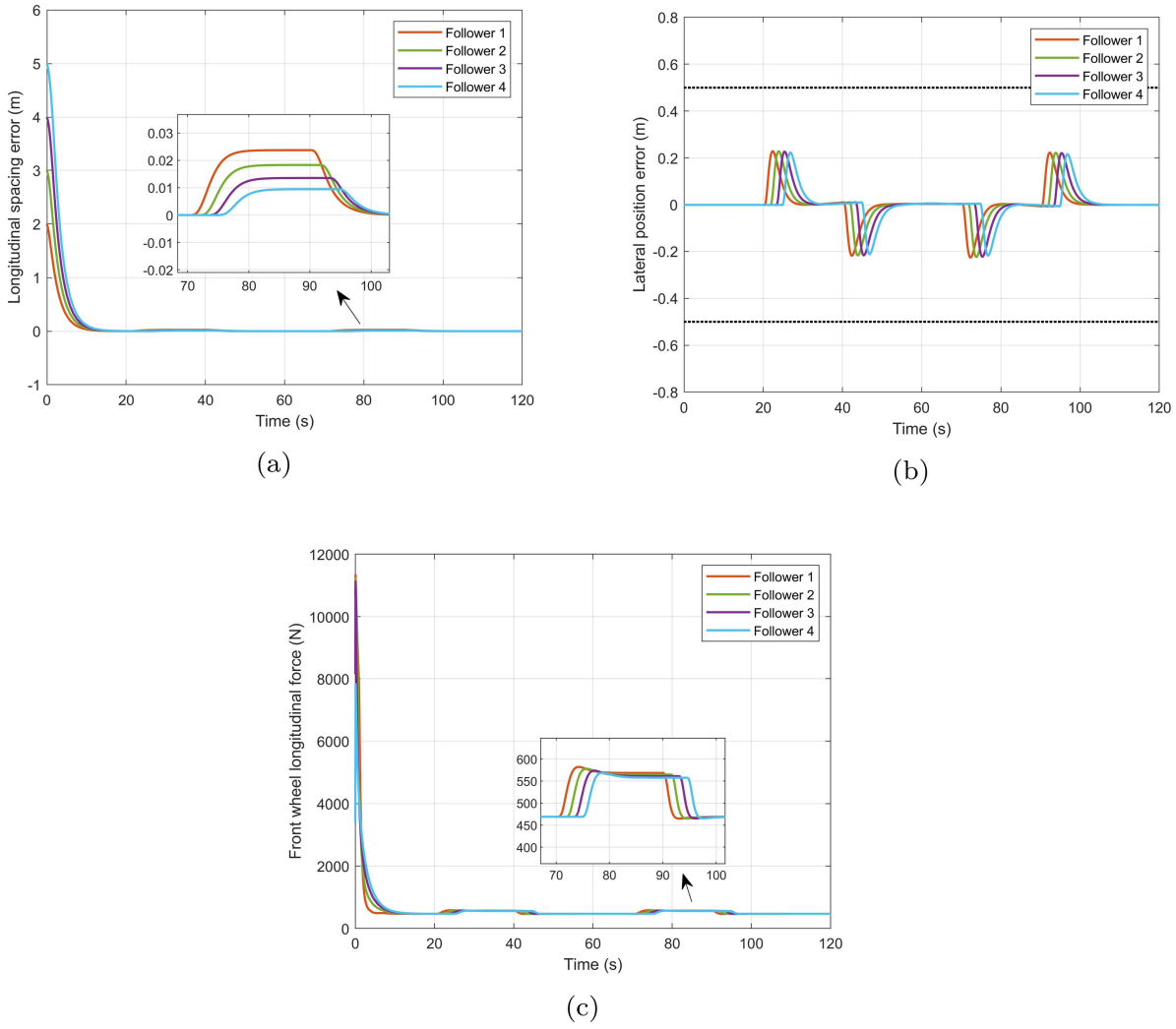

Figure 7. Truck platoon in scenario 1: (a) longitudinal spacing errors, (b) lateral position errors, and (c) front wheel longitudinal forces.

Figure 6(a) illustrates the road curvature, with a maximum curvature of 0.0025. Figure 6(b) shows the phase trajectories of the following trucks in a platoon. It can be observed that the lateral velocities and yaw rates of the four following trucks ultimately converge to the origin.

Figure 6(c) illustrates that the following trucks rapidly attain a speed of 25 m/s, matching that of the leading truck, from an initial speed of 23 m/s. Figure 7(a) illustrates that the longitudinal spacing errors rapidly converge to zero from their initial values. It can be observed that the first following truck demonstrates the maximum longitudinal spacing error of about 0.025 m. The longitudinal spacing errors of the other following trucks are also decreasing, which is consistent with the control objective of maintaining the desired distance.

It can be observed from the Figure 7(b) that the maximum errors between the lateral positions of the four following trucks and the road centreline is approximately 0.22 m, which is below the allowable error of 0.5 m. The lateral control objective of the platoon has been met.

Figures 7(c) to 8(c) show the diagrams of longitudinal tire forces and lateral tire forces of the following trucks. It can be seen that the maximum longitudinal force and the maximum lateral force of the front tires are approximately 580 N and 9000 N, the maximum longitudinal force and the maximum lateral force of the rear tires are approximately 1350 N and 15,000 N. Therefore, considering the tire force constraints, one has:

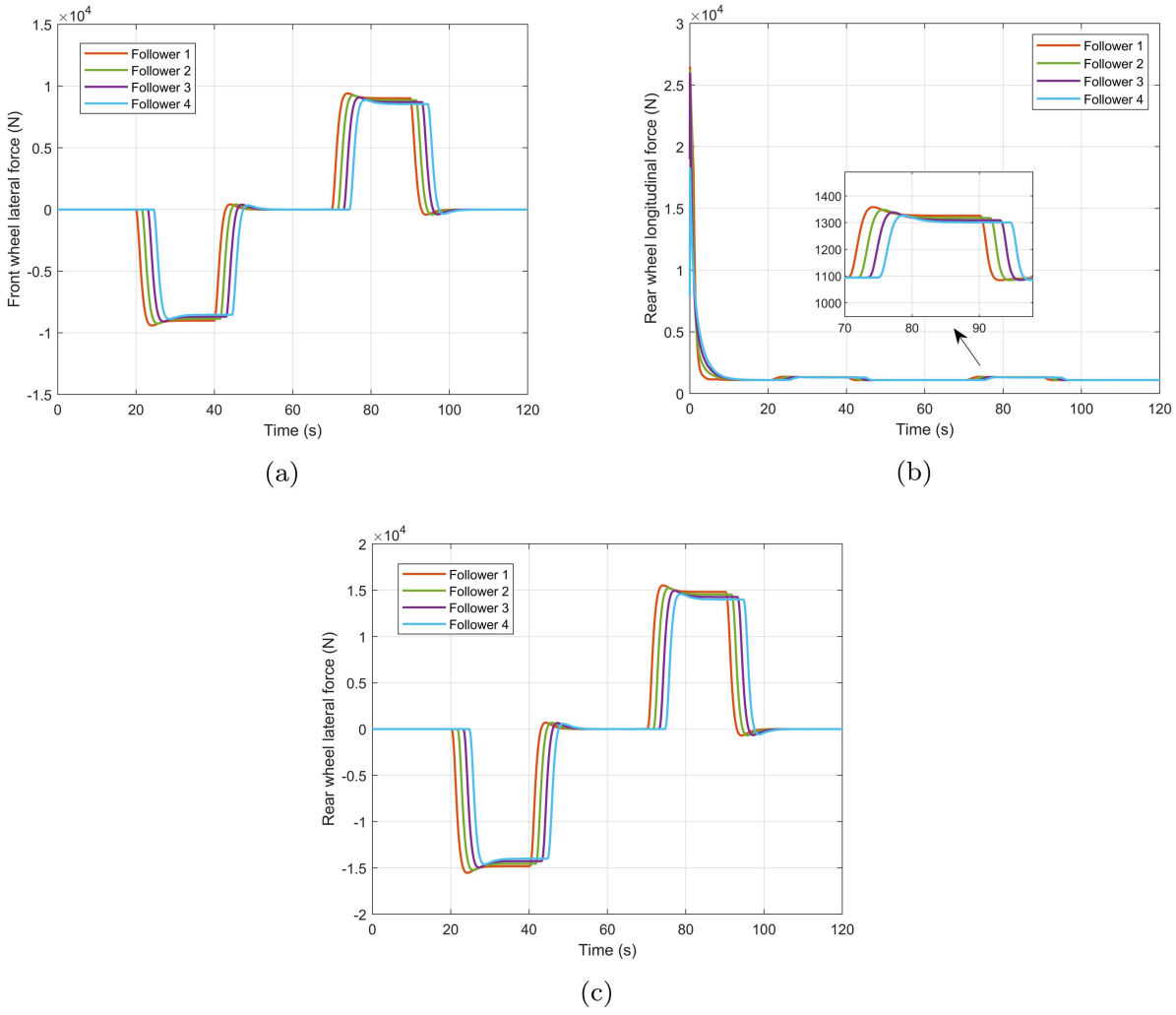

Figure 8. Truck platoon in scenario 1: (a) front wheel lateral forces, (b) rear wheel longitudinal forces, and (c) rear wheel lateral forces.

$$\begin{cases} \sqrt{F_{xf,\max}^2 + F_{yf,\max}^2} \approx 9019\text{N} < \mu F_{zf} \approx 44982\text{N} \\ \sqrt{F_{xr,\max}^2 + F_{yr,\max}^2} \approx 15061\text{N} < \mu F_{zr} \approx 104958\text{N} \end{cases}. \tag{60}$$

According to Equation (60), the longitudinal and lateral tire forces of the front and rear wheels are well below the constraint of the tire force. Therefore, the safety of the platoon will be ensured.

Under the proposed hierarchical control scheme for lateral and longitudinal coupling of the truck platoon, the platoon can maintain a safe driving state at a high speed.

4.2 Scenario 2: sinusoidal curvature

In this section, the road curvature that varies continuously with time is used as a disturbance, and a sinusoidal road condition is selected as a simulation scenario, which can be described as:

$$Y = 100 \sin\left(\frac{X}{300}\pi\right), \tag{61}$$

where Y and X are the lateral position and the longitudinal position, respectively.

The mathematical expression for road curvature is:

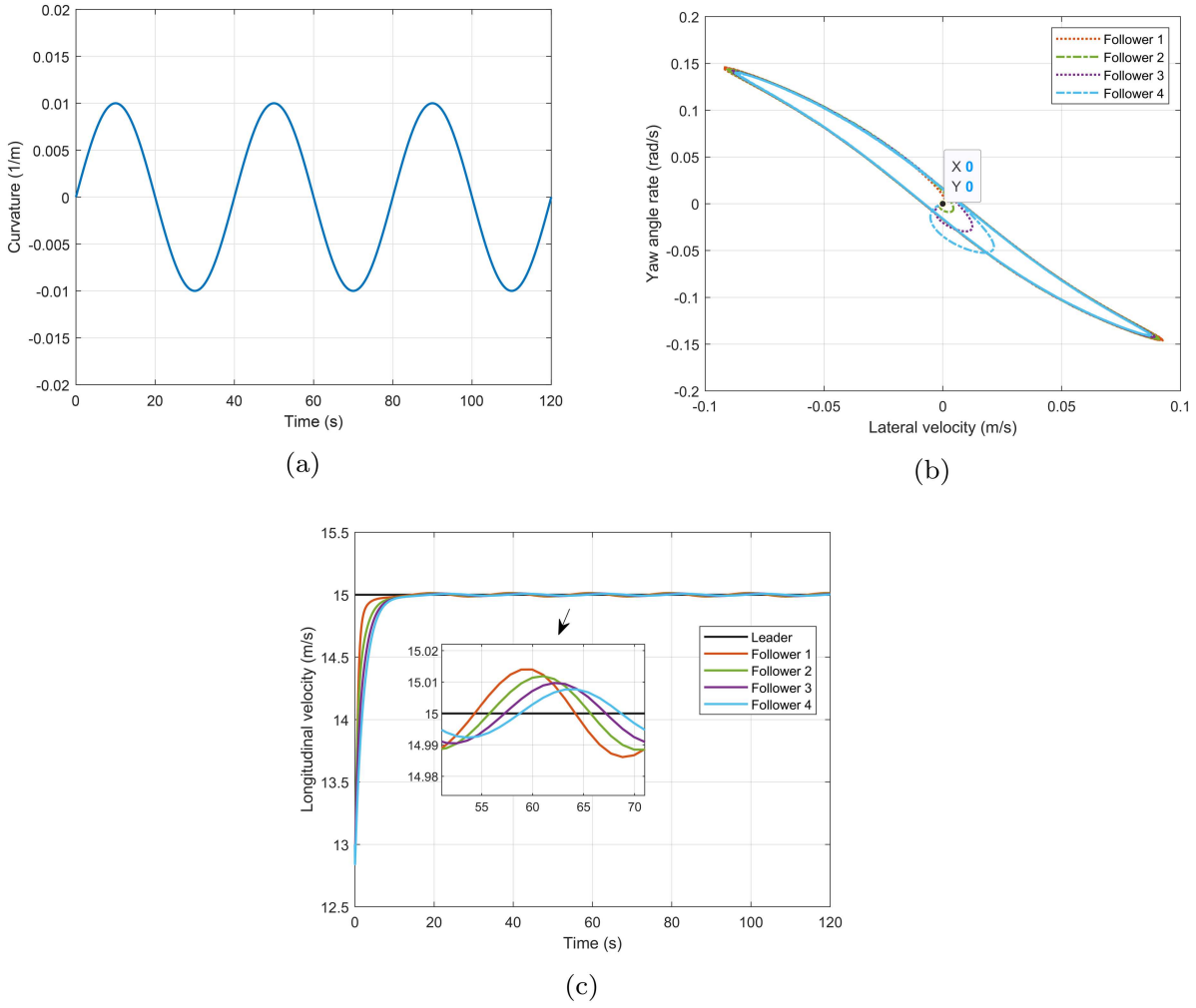

Figure 9. Truck platoon in scenario 2: (a) road curvature, (b) phase trajectories, and (c) longitudinal velocities.

$$K = \frac{|\ddot{Y}|}{(1 + \dot{Y}^2)^{1.5}}. \tag{62}$$

Combining Equations (61) and (62), the curvature of the simulated road is:

$$K = 0.01 \sin\left(\frac{v_x}{300}\pi t\right). \tag{63}$$

The maximum road curvature of 0.01 and the road surface adhesion coefficient of 0.85 are selected. The leading truck is set to travel at a constant speed of 15 m/s, and the initial speed of the following trucks is 13 m/s. The initial longitudinal spacing errors between the leading truck and the four following trucks are set as 2, 3, 4, and 5 m, respectively. The initial lateral position errors and yaw angle errors of the trucks are 0. The simulation results are shown in Figures 9–11.

Figure 9(a) illustrates the road curvature, with a maximum curvature of 0.01. From the Figure 9(b), it can be observed that the phase trajectories of the following trucks exhibit minor fluctuations in response to a continuous change in road curvature. This finding indicates that the proposed hierarchical control structure for the lateral and longitudinal coupled truck platoon is robust to disturbances.

Figures 9(c) and 10(a) show the longitudinal velocities and longitudinal spacing errors of the platoon, it can be observed that as the curvature of the road surface undergoes continuous variation, the longitudinal velocities and longitudinal spacing errors of the following trucks consequently fluctuate within the permissible limits. Figure 9(c) illustrates that the following trucks rapidly attain a speed of 15 m/s, matching

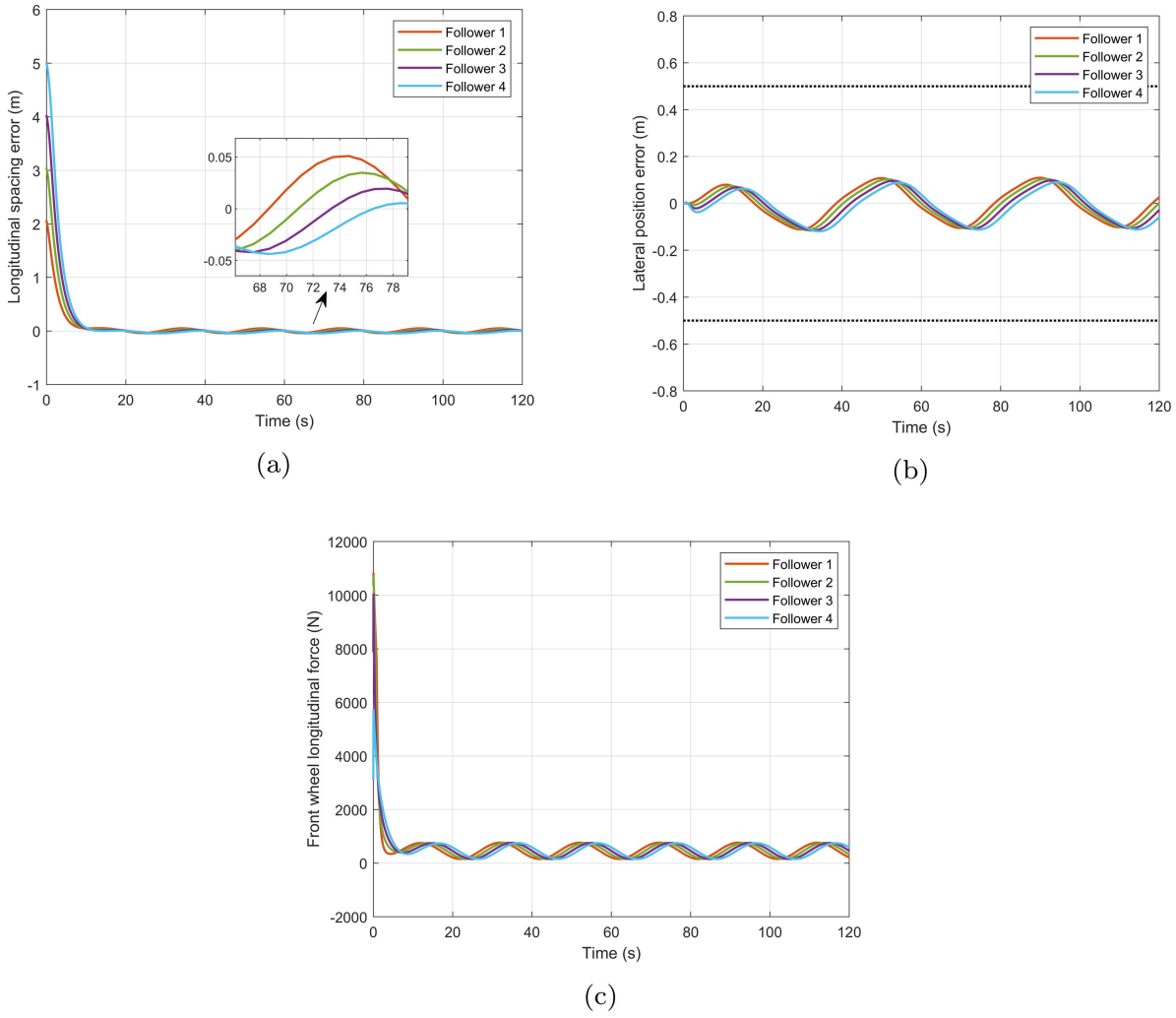

Figure 10. Truck platoon in scenario 2: (a) longitudinal spacing errors, (b) lateral position errors, and (c) front wheel longitudinal forces.

that of the leading truck, from an initial speed of 13 m/s. Figure 10(a) shows that the longitudinal spacing errors of the platoon still fluctuate at 0 under sinusoidal conditions with continuous curvature changes. It can be observed that the longitudinal spacing error of the first following truck is the greatest, reaching approximately 0.05 m. The longitudinal spacing errors of the other following trucks are also decreasing in turn, which is consistent with the control objective of maintaining the desired distance.

Figure 10(b) illustrates the lateral position errors of the following trucks. It can be observed from the figure that the maximum errors between the lateral positions of the four following trucks and the road centreline during the platoon travelling is approximately 0.1 m, which is below the allowable error of 0.5 m stipulated in this paper. Consequently, the lateral control objective of the platoon has been met.

Figures 10(c) to 11(c) show the diagrams of the longitudinal tire forces and lateral tire forces of the following trucks. It can be seen that the maximum longitudinal force and the maximum lateral force of the front tires are approximately 800 N and 19,000 N, the maximum longitudinal force and the maximum lateral force of the rear tires are approximately 2000 N and 32,000 N. Therefore, considering the tire force constraints, one has:

$$\begin{cases} \sqrt{F_{xf,\max}^2 + F_{yf,\max}^2} \approx 19017\text{N} < \mu F_{zf} \approx 44982\text{N} \\ \sqrt{F_{xr,\max}^2 + F_{yr,\max}^2} \approx 32062\text{N} < \mu F_{zr} \approx 104958\text{N} \end{cases}. \tag{64}$$

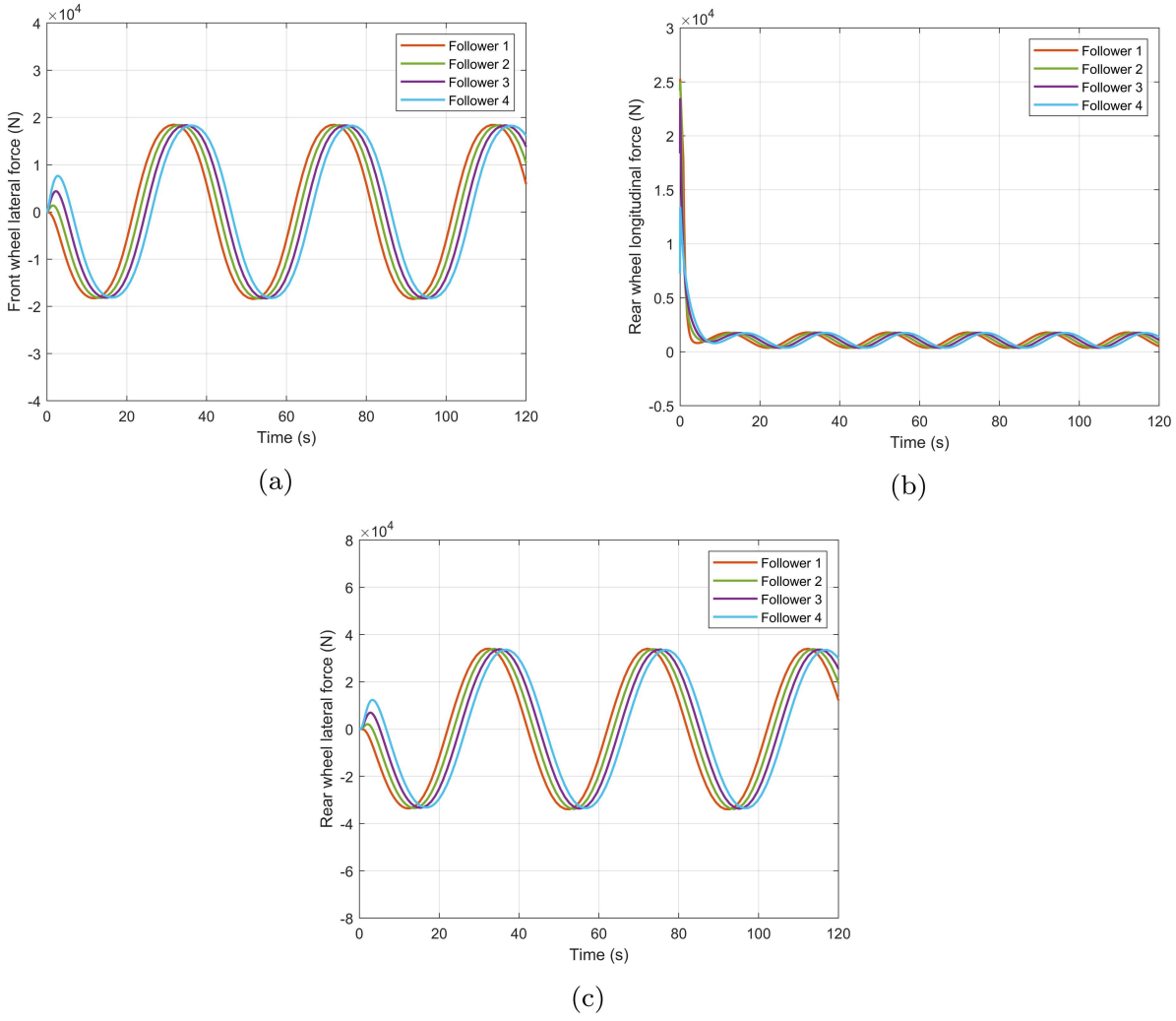

Figure 11. Truck platoon in scenario 2: (a) front wheel lateral forces, (b) rear wheel longitudinal forces, and (c) rear wheel lateral forces.

According to Equation (64), the longitudinal and lateral tire forces of the front and rear wheels are well below the tire force constraint limits. Therefore, the platoon will drive stably, and the safety of the platoon will be ensured.

In summary, under the effect of the proposed hierarchical control scheme for the lateral and longitudinal coupled truck platoon, the platoon can still maintain a stable driving state under sinusoidal conditions with continuous changes in road curvature, avoiding collisions between trucks and breaking away from the platoon, which demonstrates the robustness of the proposed hierarchical control scheme.

4.3 Safety analysis of the truck platoon

In order to ensure the safe travelling of the truck platoon, it is necessary to obtain the 'maximum' safe travelling velocity of the proposed hierarchical control scheme. The maximum safe driving speed reported in this study is quantitatively defined as the highest constant speed attainable by the leading truck, under which the entire platoon can operate without violating any of the following safety criteria:

1) Lateral deviation safety: the maximum absolute lateral position error of any following truck must remain below the allowable threshold of 0.5 m at all times, ensuring that the vehicle stays within the physical lane boundaries.

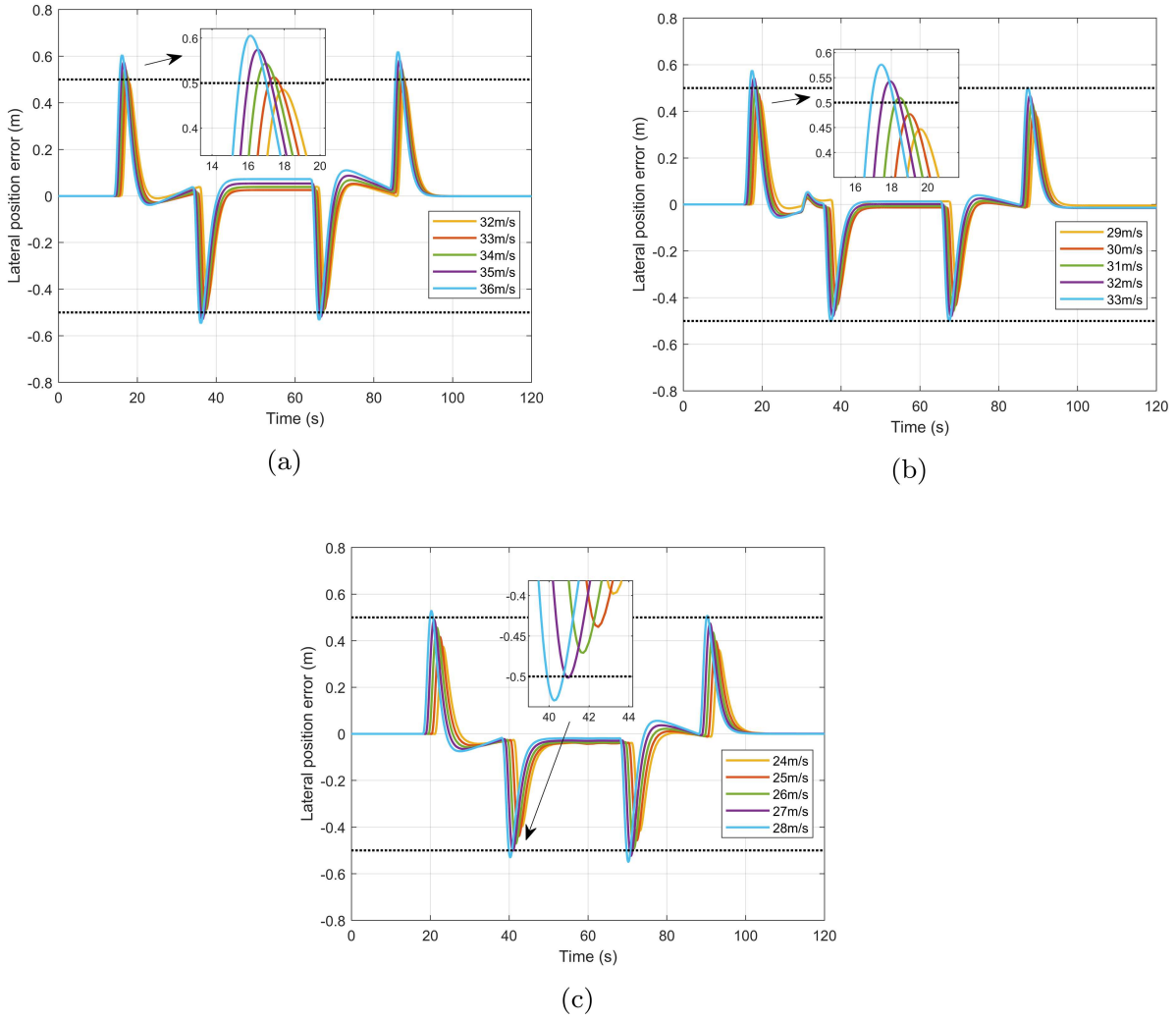

Figure 12. The lateral position errors of the first following truck in scenario 1 with three road adhesion coefficients: (a) $\mu = 0.85$, (b) $\mu = 0.60$, and (c) $\mu = 0.35$.

2) Longitudinal spacing safety: the platoon must maintain string stability. Furthermore, the combined longitudinal spacing error for all trucks must remain bounded and converge without exhibiting divergent oscillations that would risk a collision.
3) Actuator authority safety: the resultant tire force at each wheel must remain within its friction circle constraint. A violation of this constraint indicates that the tire has saturated and that the vehicle has lost the necessary force authority to maintain stable tracking.

Therefore, the safety of platoons with different road curvatures and different road surface adhesion coefficients are considered in this section.

The longitudinal velocity error of the first following truck in the platoon is the largest one due to string stability, so the first following truck is chosen as the comparison objective. The simulation conditions are as follows:

High-speed experiment: the maximum road curvature of 0.0025 and road surface adhesion coefficients of 0.85, 0.6 and 0.35 are selected, respectively. The initial longitudinal velocity error between the leading truck and the first following truck are 2 m/s, the initial longitudinal spacing error between the leading truck and the first following truck are 2 m, and the other initial errors are 0. The simulation results are shown in Figures 12 to 13.

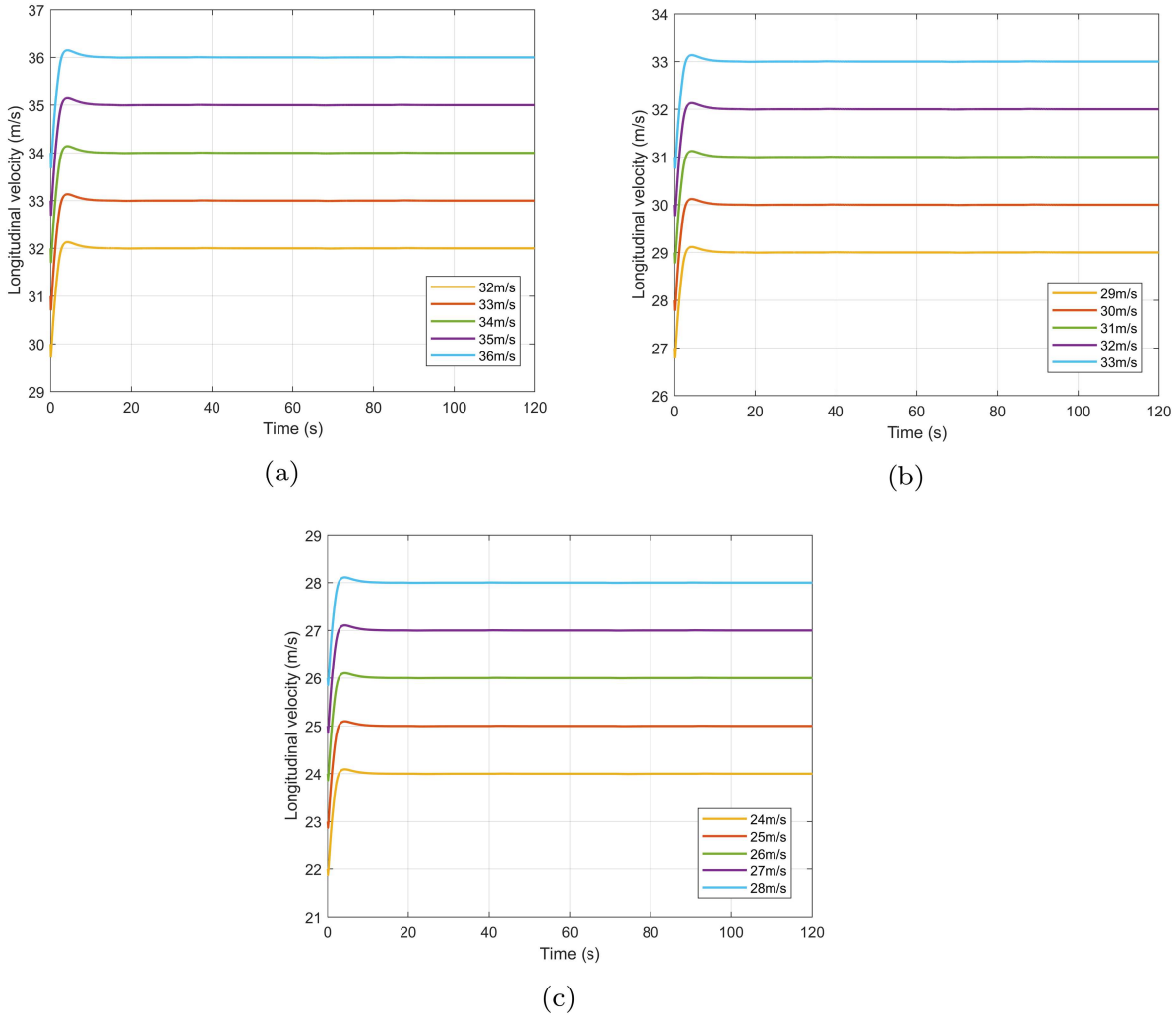

Figure 13. The longitudinal velocities of the first following truck in scenario 1 with three road adhesion coefficients: (a) $\mu = 0.85$, (b) $\mu = 0.60$, and (c) $\mu = 0.35$.

Sinusoidal curvature experiment: the maximum road curvature of 0.01 and the road surface adhesion coefficients of 0.85, 0.6 and 0.35 are selected, respectively. The initial longitudinal velocity error between the leading truck and the first following truck are 2 m/s, the initial longitudinal spacing error between the leading truck and the first following truck are 2 m, and the other initial errors are 0. The simulation results are shown in Figures 14 and 15.

Figures 12 and 13 show the lateral position errors and longitudinal velocities of the first following truck in the platoon with different road adhesion coefficients, from which it can be seen that the platoon is able to drive stably under all three types of road adhesion coefficients. The maximum safe travelling velocities of the platooning trucks are 32, 30 and 26 m/s at road adhesion coefficients of 0.85, 0.6 and 0.35, respectively.

Figures 14 and 15 show the lateral position errors and longitudinal velocities of the first following truck in the platoon under the road curvature that varying continuously with different road adhesion coefficients, from which it can be seen that the platoon is able to drive stably under all three types of road adhesion coefficients. The maximum safe travelling velocities of the platooning trucks are 20, 18 and 17 m/s at road adhesion coefficients of 0.85, 0.6 and 0.35, respectively.

The maximum safe traveling speeds for the truck platoon, obtained from the simulation analysis, are consolidated in Table 6. This table provides a clear and quantitative overview of the platoon's safe operating envelope, demonstrating how the maximum safe speed decreases with both reducing road adhesion coefficient and increasing road curvature.

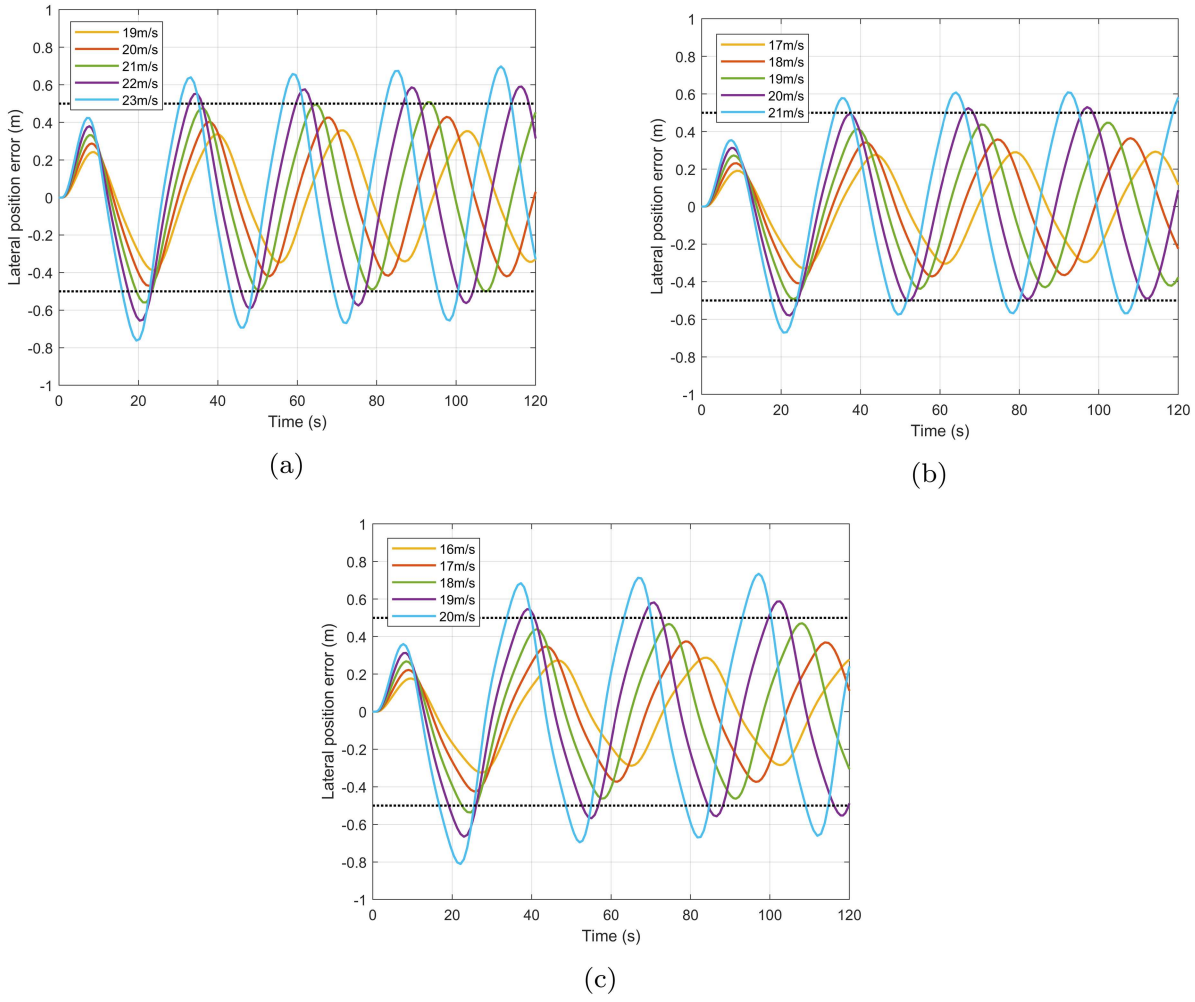

Figure 14. The lateral position errors of the first following truck in scenario 2 with three road adhesion coefficients: (a) $\mu = 0.85$, (b) $\mu = 0.60$, and (c) $\mu = 0.35$.

Remark 10. The values in Table 6 are determined through an iterative simulation process. For each combination of the road adhesion coefficient and curvature scenario, the platoon speed is systematically increased in a series of simulations. The maximum safe traveling velocity is identified as the highest speed at which the platoon could operate without violating the predefined safety criteria. A limitation of this work is that the maximum safe speed is inherently coupled to road curvature and the surface friction coefficient. Lower friction or higher curvature results in a reduced safe speed threshold.

Figures 13 and 15 show that the maximum safe travelling velocity of the truck platoon decreases when the road surface adhesion coefficient decreases. Figures 16 and 17 show that the proposed hierarchical control scheme for truck platoons is able to improve the safety threshold of the maximum travelling speed of the truck platoon compared to controllers based on longitudinal and lateral decoupled designs proposed in Yu et al. (2025a), which can ensure travelling safety of the platoon as well. Note that the method in Yu, Sun, et al. (2025) employs a fully separated control structure in which the longitudinal and lateral dynamics are regulated by two independent sliding-mode controllers. Specifically, the longitudinal controller determines the desired acceleration solely from spacing and speed errors without incorporating any dynamic coupling effects. In parallel, the lateral controller computes the steering command based exclusively on lateral deviation and yaw-rate feedback, thereby ignoring the influence of longitudinal speed variations on lateral tire forces and overall vehicle dynamics. This decoupled controller is implemented in the same Simulink-TruckSim co-simulation environment as our proposed method, ensuring that all vehicle parameters, road conditions, and initial states remained identical across tests.

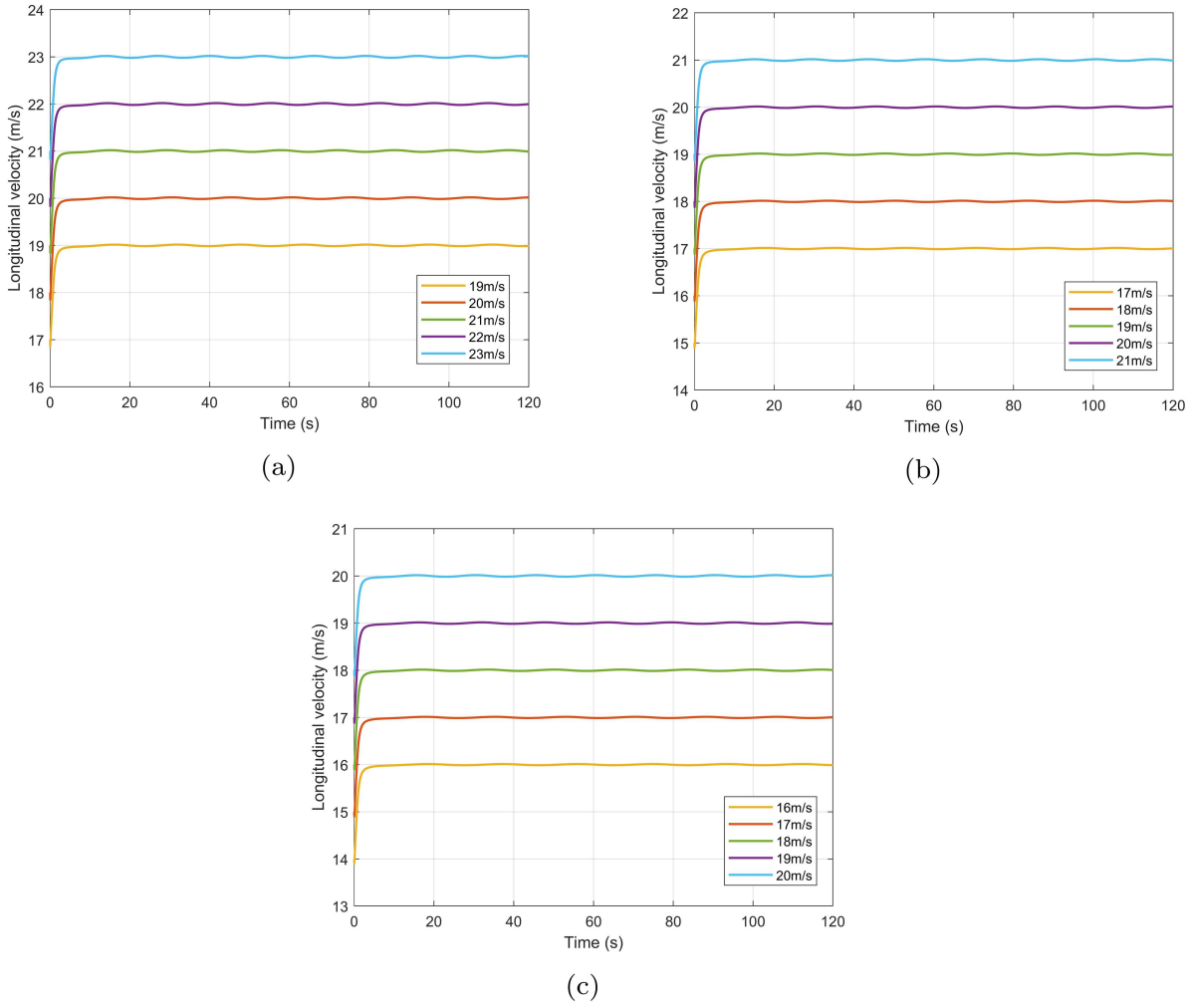

Figure 15. The longitudinal velocities of the first following truck in scenario 2 with three road adhesion coefficients: (a) $\mu = 0.85$, (b) $\mu = 0.60$, and (c) $\mu = 0.35$.

Table 6. Maximum safe traveling velocity under different operating conditions.

Road surface adhesion coefficients	Curvature of 0.0025	Curvature of 0.01
0.85	32 m/s	20 m/s
0.6	30 m/s	18 m/s
0.35	26 m/s	17 m/s

The concept of the maximum safe speed defines a safe operational envelope for the platoon, fundamentally governed by the interplay between road adhesion, curvature, and tire force constraints. The observed trends-where speed limits decrease with both reducing μ and increasing k are rooted in vehicle dynamics principles (Liu et al. 2025b). The lateral acceleration demand must be accommodated within the finite friction potential μF_z, as described by the friction ellipse. The proposed hierarchical controller actively manages this coupled longitudinal–lateral force allocation, preventing premature tire saturation and thus enabling a broader safety envelope compared to the decoupled benchmark, which neglects these interactions. These quantified results provide critical insight for defining speed policies in real-world platooning and offer practical reference values that can inform engineering deployment. Moreover, they lay the groundwork for a future real-time safety supervisor capable of dynamically adjusting the platoon speed based on road conditions.

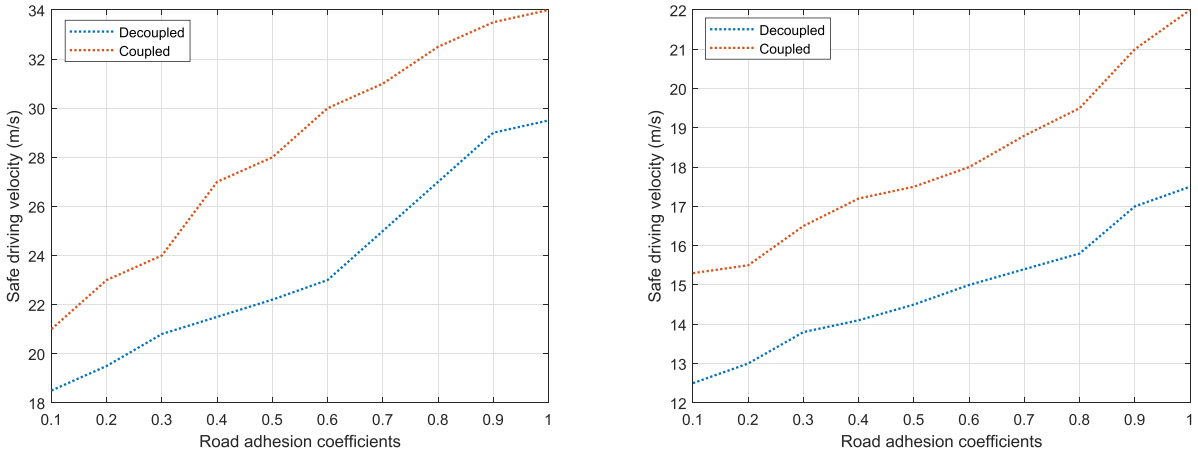

Figure 16. The maximum safe driving velocity of the truck platoon under different road adhesion coefficients: (a) road curvature of 0.0025 and (b) road curvature of 0.01.

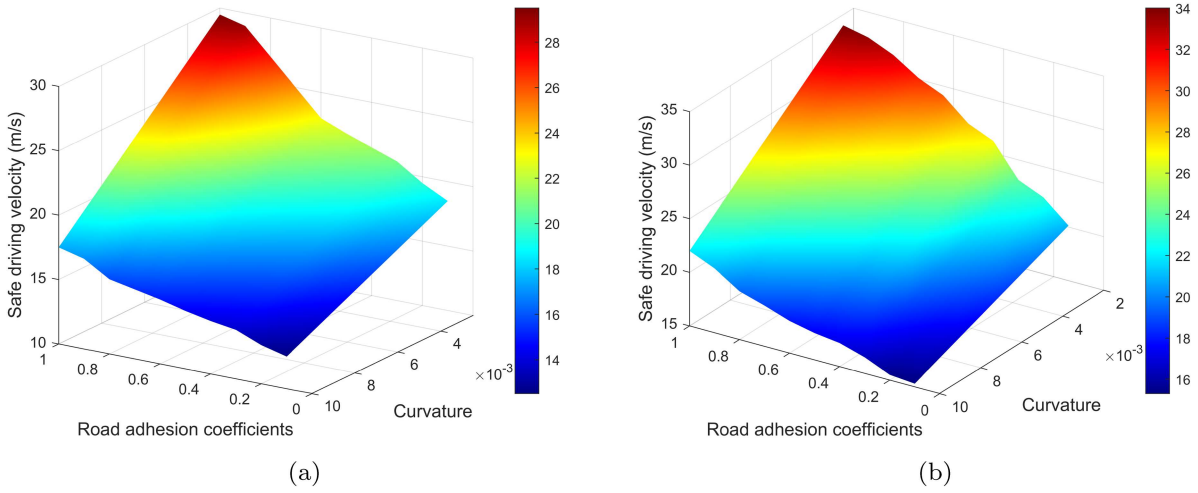

Figure 17. The maximum safe driving velocity of the truck platoon under different road adhesion coefficients and different road curvatures: (a) method in Yu, Sun, et al. (2025) and (b) method proposed in this work.

Remark 11. The maximum safe speeds reported in this section are identified through a systematic parameter search in simulation, whereby the platoon speed is increased until a violation of the predefined safety constraints occurred. This empirical approach provides a practical and comparative assessment of the safety envelope under the proposed control scheme. An avenue for future work is to establish formal safety guarantees, potentially through advanced techniques such as stability margin analysis (Xu Wang et al. 2024).

5 Conclusion

This study investigated the fundamental safety limits of truck platoons operating under curved roads and low-adhesion conditions. A hierarchical cooperative control framework was developed that explicitly incorporating longitudinal–lateral coupling and tire force saturation. Theoretical analysis and co-simulations demonstrated that the proposed strategy ensures finite-time convergence, string stability, and superior safety performance compared with conventional decoupled approaches. Most importantly, the results quantify the maximum safe driving speed of platoons across varying curvature and adhesion

coefficients, offering a systematic understanding of their operating envelope. These findings provide new insights into cooperative platoon dynamics and have direct implications for traffic safety management, infrastructure design, and the large-scale deployment of freight platooning. Future work will extend this framework to mixed traffic environments and communication-impaired scenarios, where heterogeneous vehicle behaviours pose additional challenges. Additionally, future work will include a comprehensive stochastic robustness analysis, using methods such as Monte Carlo simulations, to evaluate the controller's performance under a broader spectrum of random initial conditions, parameter uncertainties, and unmeasured disturbances.

Acknowledgements

We thank the anonymous reviewers for constructive comments.

Author contributions

None.

Disclosure statement

No potential conflict of interest was reported by the author(s).

Funding

This work is supported by the Natural Science Foundation of Jilin Province (No. 20240402079GH) and the National Natural Science Foundation of China (No. 62473167).

References

Aghababa, Mohammad Pourmahmood and Mehrdad Saif. 2020. "Finite Time Sliding Mode Control of Connected Vehicle Platoons Guaranteeing String Stability." In *2020 IEEE International Conference on Human-Machine Systems (ICHMS)*, edited by Fortino Giancarlo. 1–6, New York: IEEE. https://doi.org/10.1109/ICHMS49158.2020.9209466.

Ali, Alan, Gaetan Garcia, and Philippe Martinet. 2013. "Minimizing the Inter-Vehicle Distances of the Time Headway Policy for Urban Platoon Control with Decoupled Longitudinal and Lateral Control." In *16th International IEEE Conference on Intelligent Transportation Systems (ITSC 2013)*, edited by Hegyi Andreas and De Schutter Bart. 1805–1810, New York: IEEE. https://doi.org/10.1109/ITSC.2013.6728490.

Alonso, Marta, Daniel A Mántaras, and Pablo Luque. 2019. "Toward a Methodology to Assess Safety of a Vehicle." *Safety Science* 119: 133–140. https://doi.org/10.1016/j.ssci.2019.01.012.

Barbaro, Mario, Andrea Genovese, Francesco Timpone, and Aleksandr Sakhnevych. 2024. "Extension of the Multiphysical Magic Formula Tire Model for Ride Comfort Applications." *Nonlinear Dynamics* 112 (6): 4183–4208. https://doi.org/10.1007/s11071-023-09266-0.

Chen, Bo, Ruiqing Ma, Yang Zhou, Rui Ma, Wentao Jiang, and Fan Yang. 2024. "Co-optimization of Speed Planning and Cost-Optimal Energy Management for Fuel Cell Trucks under Vehicle-Following Scenarios." *Energy Conversion and Management* 300: 117914. https://doi.org/10.1016/j.enconman.2023.117914.

Cui, Yukang, Yiwen Liang, Qianyue Luo, Zhan Shu, and Tingwen Huang. 2024. "Resilient Consensus Control of Heterogeneous Multi-Uav Systems with Leader of Unknown Input against Byzantine Attacks." *IEEE Transactions on Automation Science and Engineering* 22: 5388–5399. https://doi.org/10.1109/TASE.2024.3420697.

Dai, Yulu, Chen Wang, and Yuanchang Xie. 2024. "Safety-Oriented Automated Vehicle Longitudinal Control Considering Both Stability and Damping Behavior." *Accident Analysis & Prevention* 198: 107486. https://doi.org/10.1016/j.aap.2024.107486.

Dell'Orto, G., G. Mastinu, R. Happee, and J. K. Moore. 2024. "Measurement of the Lateral Characteristics and Identification of the Magic Formula Parameters of City and Cargo Bicycle Tyres." *Vehicle System Dynamics* 63: 1–25. https://doi.org/10.1080/00423114.2024.2338143.

Ding, Wenhao, Chejian Xu, Mansur Arief, Haohong Lin, Bo Li, and Ding Zhao. 2023. "A Survey on Safety-Critical Driving Scenario generation-a Methodological Perspective." *IEEE Transactions on Intelligent Transportation Systems* 24 (7): 6971–6988. https://doi.org/10.1109/TITS.2023.3259322.

Feng, Yangyang, Shuyou Yu, Encong Sheng, Yongfu Li, Shuming Shi, Jianhua Yu, and Hong Chen. 2023a. "Distributed Mpc of Vehicle Platoons Considering Longitudinal and Lateral Coupling." *IEEE Transactions on Intelligent Transportation Systems* 25 (3): 2293–2310. https://doi.org/10.1109/TITS.2023.3323478.

Feng, Yangyang, Shuyou Yu, Hao Chen, Yongfu Li, Shuming Shi, Jianhua Yu, and Hong Chen. 2023b. "Distributed Mpc of Vehicle Platoons with Guaranteed Consensus and String Stability." *Scientific Reports* 13 (1): 10396. https://doi.org/10.1038/s41598-023-36898-4.

Gambhire, S. J., D Ravi Kishore, P. S. Londhe, and S. N. Pawar. 2021. "Review of Sliding Mode Based Control Techniques for Control System Applications." *International Journal of Dynamics and Control* 9 (1): 363–378. https://doi.org/10.1007/s40435-020-00638-7.

Goli, Mohammad and Azim Eskandarian. 2019. "Mpc-Based Lateral Controller with Look-Ahead Design for Autonomous Multi-Vehicle Merging into Platoon." In *2019 American Control Conference (ACC)*, edited by Lawrence Douglas and Serrani Andrea. 5284–5291. IEEE. https://doi.org/10.23919/ACC.2019.8814967.

Guo, Ge, and Z. W. Zhao. 2023. "Finite-Time Terminal Sliding Mode Control of Connected Vehicle Platoons." *Control Theory & Applications* 40 (1): 149–159.

Guo, Jinghua, Keqiang Li, and Yugong Luo. 2015. "Coordinated Control of Autonomous Four Wheel Drive Electric Vehicles for Platooning and Trajectory Tracking Using a Hierarchical Architecture." *Journal of Dynamic Systems, Measurement, and Control* 137 (10): 101001. https://doi.org/10.1115/1.4030720.

Hashemi, Ehsan, and Amir Khajepour. 2024. "Integrated Path-Tracking and Combined-Slip Force Controls of Autonomous Ground Vehicles with Safe Constraints Adaptation." *IEEE Transactions on Intelligent Vehicles* 9 (3): 4265–4274. https://doi.org/10.1109/TIV.2024.3367815.

Hong, Yigwruang, Jie Huang, and Yangsheng Xu. 2001. "On an Output Feedback Finite-Time Stabilization Problem." *IEEE Transactions on Automatic Control* 46 (2): 305–309.

Hua, Min, Xinda Qi, Dong Chen, Kun Jiang, Zemin Eitan Liu, Hongyu Sun, Quan Zhou, and Hongming Xu. 2025. "Multi-Agent Reinforcement Learning for Connected and Automated Vehicles Control: Recent Advancements and Future Prospects." *IEEE Transactions on Automation Science and Engineering* 22: 16266–16286. https://doi.org/10.1109/TASE.2025.3574280.

Karafyllis, Iasson, Dionysios Theodosis, and Markos Papageorgiou. 2023. "Nonlinear Adaptive Cruise Control of Vehicular Platoons." *International Journal of Control* 96 (1): 147–169. https://doi.org/10.1080/00207179.2021.1982015.

Kim, Jinsoo, Jahng-Hyon Park, and Kyung-Young Jhang. 2020. "Decoupled Longitudinal and Lateral Vehicle Control Based Autonomous Lane Change System Adaptable to Driving Surroundings." *IEEE Access* 9: 4315–4334. https://doi.org/10.1109/ACCESS.2020.3047189.

Latrech, Chedia, Ahmed Chaibet, Moussa Boukhnifer, and Sébastien Glaser. 2018. "Integrated Longitudinal and Lateral Networked Control System Design for Vehicle Platooning." *Sensors*18 (9): 3085. https://doi.org/10.3390/s18093085.

Li, Yongfu, Sen Zhang, Longwang Huang, and Gang Huang. 2023. "Nonlinear Longitudinal Cooperative Control of Heterogeneous Connected Vehicle Platoon Considering Car-Following Interactions and Communication Delay." *Transportmetrica B: Transport Dynamics* 11 (1): 1687–1706. https://doi.org/10.1080/21680566.2023.2241643.

Li, Handong, Haimeng Wu, Ishita Gulati, Saleh A Ali, Volker Pickert, and Satnam Dlay. 2022. "An Improved Sliding Mode Control (Smc) Approach for Enhancement of Communication Delay in Vehicle Platoon System." *IET Intelligent Transport Systems* 16 (7): 958–970. https://doi.org/10.1049/itr2.12189.

Lian, Zhi, Peng Shi, Cheng-Chew Lim, and Xin Yuan. 2022. "Fuzzy-Model-Based Lateral Control for Networked Autonomous Vehicle Systems under Hybrid Cyber-Attacks." *IEEE Transactions on Cybernetics* 53 (4): 2600–2609. https://doi.org/10.1109/TCYB.2022.3151880.

Liang, Yixiao, Yinong Li, Yinghong Yu, Zhida Zhang, Ling Zheng, and Yue Ren. 2021. "Path-Following Control of Autonomous Vehicles Considering Coupling Effects and Multi-Source System Uncertainties." *Automotive Innovation* 4 (3): 284–300. https://doi.org/10.1007/s42154-021-00155-z.

Liu, Jinkun. 2012. "Sliding Mode Control Design and Matlab Simulation." In *The Basic Theory and Design Method*, edited by Li X and Wang Y. 35–37, Beijing, China: Tsinghua University Press.

Liu, Yujie, Ming Yue, Xudong Zhao, and Guangdeng Zong. 2025. "Adaptive Robust Path Tracking Preview Control for Tractor-Trailer Trucks Considering Trailer Sway and Stochastic Disturbances." *IEEE Transactions on Intelligent Transportation Systems* 26 (4): 5422–5434. https://doi.org/10.1109/TITS.2024.3524581.

Liu, Jiahui, Yang Liu, Liang Wang, and Xiaobo Qu. 2025. "A Survey and Comprehensive Taxonomy of Tire-Road Adhesion Coefficient Estimation for Intelligent Vehicles." *IEEE Transactions on Intelligent Transportation Systems* 26 (9): 12819–12833. https://doi.org/10.1109/TITS.2025.3565542.

Liu, Yang, Hongyi Li, Renquan Lu, Zongyu Zuo, and Xiaodi Li. 2022. "An Overview of Finite/Fixed-Time Control and Its Application in Engineering Systems." *IEEE/CAA Journal of Automatica Sinica* 9 (12): 2106–2120. https://doi.org/10.1109/JAS.2022.105413.

Luo, Jie, Defeng He, Wei Zhu, and Haiping Du. 2022. "Multiobjective Platooning of Connected and Automated Vehicles Using Distributed Economic Model Predictive Control." *IEEE Transactions on Intelligent Transportation Systems* 23 (10): 19121–19135. https://doi.org/10.1109/TITS.2022.3170977.

Manuel, Calequela JT, Giane G Lenzi, Max MD Santos, and Angelo M Tusset. 2022. "Predictive Control Applied to the Steering System of an Autonomous Vehicle." *Journal of Vibration Engineering & Technologies* 10 (6): 2275–2282. https://doi.org/10.1007/s42417-022-00551-7.

Na, Xiaoxiang, and David J Cole. 2022. "Experimental Evaluation of a Game-Theoretic Human Driver Steering Control Model." *IEEE Transactions on Cybernetics* 53 (8): 4791–4804. https://doi.org/10.1109/TCYB.2022.3140362.

Oriol, Laura, Margarita Martínez-Díaz, Seshadri Naik Moode, Marcel Sala, and Francesc Soriguera. 2024. "Platooning of Connected Automated Vehicles on Freeways: A Microsimulation Approach." *Transportmetrica B: Transport Dynamics* 12(1): 2360543.

Qiao, Lei, and Weidong Zhang. 2019. "Trajectory Tracking Control of Auvs Via Adaptive Fast Nonsingular Integral Terminal Sliding Mode Control." *IEEE Transactions on Industrial Informatics* 16 (2): 1248–1258. https://doi.org/10.1109/TII.2019.2949007.

Rajamani, Rajesh, Han-Shue Tan, Boon Kait Law, and Wei-Bin Zhang. 2000. "Demonstration of Integrated Longitudinal and Lateral Control for the Operation of Automated Vehicles in Platoons." *IEEE Transactions on Control Systems Technology* 8 (4): 695–708.

Shi, Shuming, Ling Li, Xianbin Wang, Hongfei Liu, and Yuqiong Wang. 2017. "Analysis of the Vehicle Driving Stability Region Based on the Bifurcation of the Driving Torque and the Steering Angle." *Proceedings of the Institution of Mechanical Engineers, Part D: Journal of Automobile Engineering* 231 (7): 984–998. https://doi.org/10.1177/0954407017701554.

Sun, Yumei, Bing Chen, Chong Lin, and Honghong Wang. 2017. "Finite-Time Adaptive Control for a Class of Nonlinear Systems with Nonstrict Feedback Structure." *IEEE Transactions on Cybernetics* 48 (10): 2774–2782. https://doi.org/10.1109/TCYB.2017.2749511.

Sun, Lishan, Zeyu Cheng, Dewen Kong, Yan Xu, Shangwu Wen, and Kangyu Zhang. 2023. "Modeling and Analysis of Human-Machine Mixed Traffic Flow Considering the Influence of the Trust Level Toward Autonomous Vehicles." *Simulation Modelling Practice and Theory* 125: 102741. https://doi.org/10.1016/j.simpat.2023.102741.

Sundarapandian, Vaidyanathan and Chang-Hua Lien. 2017. *Applications of Sliding Mode Control in Science and Engineering*. Vol. 709. Cham: Springer.

Wang, Jianmei, Xiaoyuan Luo, Li Wang, Zhiqiang Zuo, and Xinping Guan. 2019. "Integral Sliding Mode Control Using a Disturbance Observer for Vehicle Platoons." *IEEE Transactions on Industrial Electronics* 67 (8): 6639–6648. https://doi.org/10.1109/TIE.2019.2936990.

Wen, Shixi, and Ge Guo. 2021. "Distributed Trajectory Optimization and Sliding Mode Control of Heterogenous Vehicular Platoons." *IEEE Transactions on Intelligent Transportation Systems* 23 (7): 7096–7111. https://doi.org/10.1109/TITS.2021.3066688.

Xiao, Lingyun, and Feng Gao. 2011. "Practical String Stability of Platoon of Adaptive Cruise Control Vehicles." *IEEE Transactions on Intelligent Transportation Systems* 12 (4): 1184–1194.

Xu, Linhai, Yingzhou Wang, Hongbin Sun, Jingmin Xin, and Nanning Zheng. 2015. "Integrated Longitudinal and Lateral Control for Kuafu-Ii Autonomous Vehicle." *IEEE Transactions on Intelligent Transportation Systems* 17 (7): 2032–2041. https://doi.org/10.1109/TITS.2015.2498170.

Xu, Liwei, Weichao Zhuang, Guodong Yin, Chentong Bian, and Huawei Wu. 2019. "Modeling and Robust Control of Heterogeneous Vehicle Platoons on Curved Roads Subject to Disturbances and Delays." *IEEE Transactions on Vehicular Technology* 68 (12): 11551–11564. https://doi.org/10.1109/TVT.2019.2941396.

Wang, Xu, Chuan Xu, Xinyu Zhao, Haibo Li, and Xinguo Jiang. 2024. "Stability and Safety Analysis of Connected and Automated Vehicle Platoon Considering Dynamic Communication Topology." *IEEE Transactions on Intelligent Transportation Systems* 25(10): 13442–13452. https://doi.org/10.1109/TITS.2024.3398111.

Yanjun, Shen, and Yuehua Huang. 2009. "Uniformly Observable and Globally Lipschitzian Nonlinear Systems Admit Global Finite-Time Observers." *IEEE Transactions on Automatic Control* 54 (11): 2621–2625. https://doi.org/10.1109/TAC.2009.2029298.

Yu, Hwapyeong, and Hwasoo Yeo. 2025. "Impact of Commercial Adaptive Cruise Control on Highway Traffic Congestion and Safety." *Transportmetrica B: Transport Dynamics* 13 (1): 2519630. https://doi.org/10.1080/21680566.2025.2519630.

Yu, Shuyou, Encong Sheng, Yajing Zhang, Yongfu Li, Hong Chen, and Yi Hao. 2022. "Efficient Nonlinear Model Predictive Control of Automated Vehicles." *Mathematics* 10 (21): 4163. https://doi.org/10.3390/math10214163.

Yu, Shuyou, Shaoyu Sun, Boqun Zhang, Hong Chen, Yongfu Li, and Baojun Lin. 2025. "Longitudinal and Lateral Control of Truck Platoons Based on Finite-Time Sliding Mode." *Proceedings of the Institution of Mechanical Engineers, Part D: Journal of Automobile Engineering* 239(14): 7090–7107. https://doi.org/10.1177/09544070241309401.

Yu, Shuyou, Zepeng Liu, Yunyong Li, Hong Chen, and Qifang Liu. 2025. "Distributed Iterative Reinforcement Learning Predictive Control of Truck Platoons." *Proceedings of the Institution of Mechanical Engineers, Part D: Journal of Automobile Engineering*, 09544070251351672.

Yu, Weijie, Xuedong Hua, and Wei Wang. 2023. "Stability and Capacity for Heterogeneous Traffic Flow Mixed with Vehicles in Multiple Controls." *Transportmetrica B: Transport Dynamics* 11 (1): 649–682. https://doi.org/10.1080/21680566.2022.2113476.

Zhang, Hui, Rongrong Wang, and Junmin Wang. 2023. "Robust Lateral Motion Control of Four-Wheel Independently Actuated Electric Vehicles with Tire Force Saturation Consideration." In *Robust Gain-Scheduled Estimation and Control of Electrified Vehicles via LPV Technique*, edited by J Wang and Y Zhang173–201, Singapore: Springer. https://doi.org/10.1007/978-981-19-8509-6_7.

Zhang, Ying, Zhaoyang Ai, Jinchao Chen, Tao You, Chenglie Du, and Lei Deng. 2021. "Energy-Saving Optimization and Control of Autonomous Electric Vehicles with Considering Multiconstraints." *IEEE Transactions on Cybernetics* 52 (10): 10869–10881. https://doi.org/10.1109/TCYB.2021.3069674.

Zhao, Wencai, Jiang Zhang, Jinxing Lai, Xinghao Shi, and Zexin Xu. 2023. "Skid Resistance of Cement Concrete Pavement in Highway Tunnel: A Review." *Construction and Building Materials* 406: 133235. https://doi.org/10.1016/j.conbuildmat.2023.133235.

Zhou, Anye, Hao Zhou, Jorge Laval, and Srinivas Peeta. 2025. "String Instability Mitigation of Adaptive Cruise Control Without Modifying Control Laws: Trajectory Shaper and Parameter Estimation." *Transportmetrica B: Transport Dynamics* 13 (1): 2473885.

Zhou, Xingyu, Heran Shen, Zejiang Wang, Hyunjin Ahn, and Junmin Wang. 2023. "Driver-Centric Lane-Keeping Assistance System Design: A Noncertainty-Equivalent Neuro-Adaptive Control Approach." *IEEE/ASME Transactions on Mechatronics* 28 (6): 3017–3028. https://doi.org/10.1109/TMECH.2023.3236245.

Zhu, Yongxin, Yongfu Li, Keyue Zeng, Longwang Huang, Gang Huang, Wei Hua, Yibing Wang, and Xinbo Gao. 2024. "Finite-Time Cooperative Control for Vehicle Platoon with Sliding-Mode Controller and Disturbance Observer." *IEEE Transactions on Intelligent Transportation Systems* 25 (9): 10679–10688. https://doi.org/10.1109/TITS.2024.3418631.

Zuo, Lei, Xiao-xue Peng, Ming-jun Cheng, and Zhuo Zhang. 2025. "Optimal Integral Sliding-Mode Based Nonlinear Vehicle Platoon Tracking Control with Directed Communication Topology and External Disturbance." *Nonlinear Dynamics* 113: 18107–18119. https://doi.org/10.1007/s11071-025-11212-1.